

BURIED FIBER OPTIC INTRUSION SENSOR

A Thesis

by

ERIC WILLIAM MAIER

Submitted to the Office of Graduate Studies of
Texas A&M University
in partial fulfillment of the requirements for the degree of

MASTER OF SCIENCE

May 2004

Major Subject: Electrical Engineering

BURIED FIBER OPTIC INTRUSION SENSOR

A Thesis

by

ERIC WILLIAM MAIER

Submitted to Texas A&M University
in partial fulfillment of the requirements
for the degree of

MASTER OF SCIENCE

Approved as to style and content by:

Henry F. Taylor
(Chair of Committee)

Chin B. Su
(Member)

Philip R. Hemmer
(Member)

John W. Poston Sr.
(Member)

Chanan Singh
(Head of Department)

May 2004

Major Subject: Electrical Engineering

ABSTRACT

Buried Fiber Optic Intrusion Sensor. (May 2004)

Eric William Maier, B.S., Texas A&M University

Chair of Advisory Committee: Dr. Henry Taylor

A distributed fiber optic intrusion sensor capable of detecting intruders from the pressure of their weight on the earth's surface was investigated in the laboratory and in field tests. The presence of an intruder above or in proximity to the buried sensor induces a phase shift in light propagating along the fiber which allows for the detection and localization of intrusions. Through the use of an ultra-stable erbium-doped fiber laser and phase sensitive optical time domain reflectometry, disturbances were monitored in long (several km) lengths of optical fiber. Narrow linewidth and low frequency drift in the laser were achieved through a combination of optical feedback and insulation of the laser cavity against environmental effects. The frequency drift of the laser, characterized using an all-fiber Mach Zehnder interferometer, was found to be less than 1 MHz/min, as required for operation of the intrusion detection system.

Intrusions were simulated in a laboratory setting using a piezoelectric transducer to produce a controllable optical phase shift at the 2 km point of a 12 km path length. Interrogation of the distributed sensor was accomplished by repetitively gating light pulses from the stable laser into the sensing fiber. By monitoring the Rayleigh backscattered light with a photodetector and comparing traces with and without an induced phase shift, the phase disturbances were detected and located. Once the

feasibility of such a sensor was proven in the laboratory, the experimental set up was transferred to Texas A&M's Riverside Campus. At the test site, approximately 40 meters of fiber optic cable were buried in a triangle perimeter and then spliced into the 12 km path length which was housed inside the test facility. Field tests were conducted producing results comparable to those found in the laboratory. Intrusions over this buried fiber were detectable on the ϕ -OTDR trace and could be localized to the intrusion point. This type of sensor has the potential benefits of heightened sensitivity, covertness, and greatly reduced cost over the conventional seismic, acoustic, infrared, magnetic, and fiber optic sensors for monitoring long (multi-km) perimeters.

To My Loving Wife and Family

ACKNOWLEDGEMENTS

I would like to express my greatest thanks and gratitude to Dr. Henry Taylor for his guidance and counsel throughout the entire research process. I would also like to express my appreciation to Dr. Philip Hemmer, Dr. Chin Su, and Dr. John Poston for volunteering their time to serve on my graduate committee. This research would not have been possible without the assistance and support of the members of this committee.

I would also like to thank Robert Atkins for his work in the laboratories and for his preparation of the Riverside test facility for our department and to Tammy Carda for her continual administrative assistance. Special thanks go to Juan Juarez for his leadership and guidance throughout my research. Finally, thanks to my wife and family for their patience and constant encouragement throughout the entire process.

TABLE OF CONTENTS

	Page
ABSTRACT	iii
DEDICATION	v
ACKNOWLEDGEMENTS	vi
TABLE OF CONTENTS	vii
LIST OF FIGURES	ix
 CHAPTER	
I INTRODUCTION	1
II THEORETICAL BACKGROUND.....	4
A. Optical fibers	4
B. Phase response to temperature changes in fiber	7
C. Phase shifts in a buried fiber	8
D. Rayleigh scattering in optical fibers	9
E. Mach Zehnder interferometer design	10
F. Laser linewidth	12
G. Frequency drift in lasers	13
H. Erbium doped fiber amplifiers	13
I. OTDR configuration	15
J. Configuration for ϕ -OTDR intrusion sensor.....	16
III EXPERIMENTAL PROCEDURES	20
A. Laser stabilization	20
B. Mach Zehnder fabrication	23
C. Frequency drift set up	24
D. ϕ -OTDR set up	26

CHAPTER	Page
IV RESULTS	28
A. Frequency drift results	28
B. Intrusion simulation results	38
V CONCLUSIONS AND FUTURE WORK	45
A. Conclusions	45
B. Future work	46
REFERENCES	48
APPENDIX A	50
APPENDIX B	51
VITA	52

LIST OF FIGURES

FIGURE	Page
1 Optical fiber structure	4
2 Light ray entering the core of an optical fiber	5
3 Spectral attenuation in a fused silica fiber	7
4 Rayleigh scatter in optical fiber	10
5 Unbalanced Mach Zehnder	11
6 Operation of EDFA	14
7 Optical time-domain reflectometer (OTDR)	16
8 Configuration for ϕ -OTDR intrusion sensor	17
9 Simulated dependence of range resolution on range in fiber	19
10 EDFL design	20
11 Spectral linewidth scan of EDFL	21
12 A)Laser and feedback path housing B) MZI housing.....	22
13 Mach Zehnder interferometers	24
14 Frequency drift experimental set up	25
15 ϕ -OTDR experimental set up	26
16 Frequency drift comparison of enclosed MZI vs. open over 20 seconds	29
17 Phase disturbance experienced when tapping near the box	30
18 Frequency drift 3 p.m.	31

FIGURE	Page
19 Frequency drift 10 p.m.	31
20 Frequency drift 3 a.m.	31
21 Frequency drift 6:12 a.m.	32
22 Frequency drift 6:17 a.m.	32
23 Frequency drift 6:22 a.m.	33
24 Drift rate with 0.0 Volts	34
25 Drift rate with 0.5 Volts	34
26 Drift rate with 1.0 Volts	35
27 Drift rate with 1.5 Volts	35
28 Drift rate with 2.0 Volts	36
29 Drift rate with 2.5 Volts	36
30 Drift rate with 3.0 Volts	37
31 Drift rate with 3.5 Volts	37
32 Noisy ϕ -OTDR traces	39
33 Stabilized ϕ -OTDR traces	39
34 Phase OTDR trace	41
35 Riverside Campus facility layout	42
36 Field test ϕ -OTDR, comparing traces with and without car driving over the buried fiber cable	44
37 Difference of ϕ -OTDR traces in Fig. 36 showing intrusion peak	44

CHAPTER I

INTRODUCTION

In the past several years we have seen an increasing demand for security in both the public and private sectors. Recent technological advances are bridging the gap into a more secure world and fiber optics may help lead the way. With the maturation of the telecommunications industry, fiber optic technologies have seen a boom in funding and research over the past decade. Extremely low optical loss and unprecedented bandwidth are prime reasons for the recent successes in photonics. The fibers and components developed for today's communications needs have greatly improved in performance and cost, and have become attractive candidates for sensor use. With advances in optical devices such as light sources and amplifiers, a buried fiber optic intrusion sensor of the type investigated here can be a viable candidate for a variety of perimeter-monitoring applications.

Present day intrusion monitoring systems make use of seismic, acoustic, infrared, magnetic, and fiber optic sensors which are limited to a small detection range and require the wireless transmission of data. The proposed system has advantages of covertness and long-range detection, thus distinguishing itself as an attractive alternative to its predecessors. While today's perimeter monitoring systems can be detected through visual observation of components deployed above ground or from

This thesis follows the style and format of *IEEE Journal of Lightwave Technology*.

electromagnetic emissions, the proposed system is covert in that the distributed sensing element, optical cable, is buried with no antennas needed to transmit the data.

Probably the greatest advantage of the fiber optic system investigated here is cost - one distributed sensing fiber can replace as many as 1000 conventional “point” sensors. This translates into order-of-magnitude improvements in the cost of monitoring long perimeters.

Recent world events have proved the need for enhanced security for both the country’s citizens and its physical assets. The intrusion sensor proposed here could see nearly limitless applications ranging from personal home security to the monitoring and subsequent protection of national borders. Modern day efforts for border security are often limited to manned checkpoints and surveillance patrols, which are hardly effective methods for thousands of miles of terrain. For example, the United States-Mexico border stretches 1,989 miles and is guarded by 1,950 agents at 43 points of entry [1]. As in this case, there is often simply too much distance to cover with human force and current detection efforts. Besides border protection, this intrusion sensor could be utilized for monitoring military outposts, national landmarks, prisons, nuclear facilities and countless other sensitive areas. This intrusion sensor would provide a continuous monitoring solution that could be deployed at a fraction of the cost of current methods and have the spatial resolution needed to identify points of intrusion.

Optical fibers as a physical medium are subjected to perturbations constantly either through geometrical (size, shape) or optical (refractive index, mode conversion) changes to varying extents depending on the nature of the disturbance. For

communication purposes attempts to minimize these effects are undertaken to maintain reliable signal transmission and reception. However in fiber optic sensing, these responses are deliberately enhanced so the resulting changes can be used to measure the external perturbations. Over the past several years fiber sensors have been utilized for measuring temperature, acoustic pressure, static pressure, strain, acceleration, magnetic field, and liquid flow rates. Fiber optic sensors are classified into three categories: amplitude, polarimetric and interferometric. The first, amplitude, measures light intensity and is the simplest form of detection. However, fiber optic amplitude sensors such as the conventional optical time domain reflectometer (OTDR) are not nearly sensitive enough to detect and locate an intruder from phase changes produced in a buried fiber optic cable. Polarimetric sensors use changes in the polarization of light to identify disturbances, but again, are not nearly sensitive enough for this purpose. The last method is interferometric, which monitors the phase disturbance in light. Interferometers provide the best sensitivity, but require more sophisticated monitoring techniques. The phase-sensitive optical time domain reflectometer (ϕ -OTDR) investigated here is an example of such a sensor [2].

This thesis focuses on the investigation of techniques which might lead to the realization of a buried fiber optic system which is capable of monitoring multi-km perimeters at a significantly reduced cost vs. conventional seismic, acoustic, infrared, magnetic, and fiber optic sensors. In the remaining chapters the theoretical background for the development of this sensor, the experimental procedures, results, conclusions, and recommendations for future work will be discussed.

CHAPTER II

THEORETICAL BACKGROUND

A. Optical fibers

Over the past few decades the demand for higher capacity, higher speed transmission lines for communication has fueled the expansion of the fiber optic industry. As the enabling technology for the internet and long haul communication lines, fiber optic technologies benefit us all.

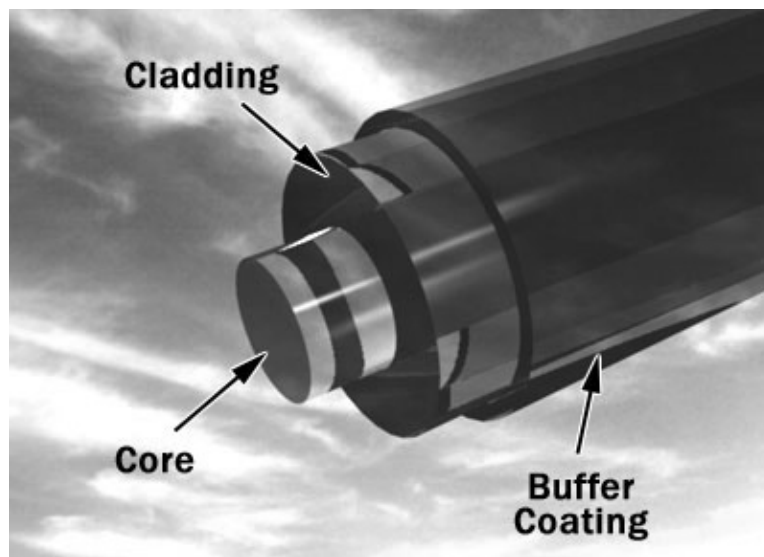


Figure 1. Optical fiber structure [3]

Optical fibers consist of three main components: the core, the cladding and the outer buffer, as shown in Figure 1. The core consists of highly pure glass, usually fused silica (SiO_2) doped with germania (GeO_2). The core is surrounded by the

cladding glass, generally pure fused silica, which has a lower refractive index than the core, as required for waveguiding. Finally an outer buffer layer made of a polymer material is used for structural integrity and protection of the underlying glass. The outer buffer, which has the highest refractive index of all the layers, generally absorbs light propagating in the cladding in a relatively short distance (tens of meters or less).

With the higher index core and lower index cladding, light coupled into the core at one end of the fiber can propagate through tens or even hundreds of km of fiber without measurable loss due to leakage into the cladding. Trapping of the light in the core is explained by the principle of total internal reflection (TIR). For a large-core multimode fiber the condition for TIR is given by $\Theta_{\text{air}} < \Theta_C$, with Θ_{air} the angle between an incident light ray and the fiber axis, and

$$\sin \Theta_C = \sqrt{n_1^2 - n_2^2} \quad (1)$$

where n_1 and n_2 are the refractive indices of the transmitting region and cladding respectively as shown in Figure 2, and it is assumed that the incident light propagates in air ($n = 1$).

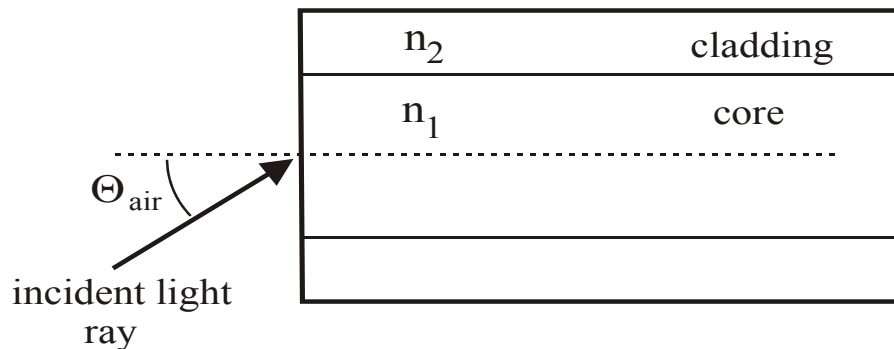


Figure 2. Light ray entering the core of an optical fiber

Optical fibers in general are divided into two main categories: single mode and multi-mode. The two types of fiber are distinguished by their relative core diameters and have different applications. Multimode fibers have much larger core diameters (50-100 μm) to allow many modes to propagate at one time, while single mode fiber cores are much smaller (8-10 μm) allowing only one mode to be transmitted. The designation of single/multimode fiber is determined by the parameter V, given by

$$V = \frac{2\pi a}{\lambda} \sqrt{n_1^2 - n_2^2}, \quad (2)$$

where a is the radius of the fiber core, λ is the wavelength, and n_1 and n_2 are the refractive indices of the core and cladding, respectively. A single mode fiber has a V-value less than 2.405, therefore anything with a larger V value is considered multimode. For interferometric sensing as in this research, single mode fibers are preferable because the propagating light wave is characterized by a single value of the phase.

An important factor in the intrusion sensor system is the fiber's attenuation. Figure 3 depicts the attenuation vs. wavelength of a single mode fused silica fiber. Attenuation peaks due to water molecules in the fiber create three main windows of operation centered around 850 nm, 1300 nm, and 1550 nm. The laser used in these experiments operates at 1555.6 nm, in the third "operational window", due to its compatibility with erbium doped fiber amplifiers (EDFAs). (It should be noted that in today's best fibers the 1380 nm water peak has been virtually eliminated.)

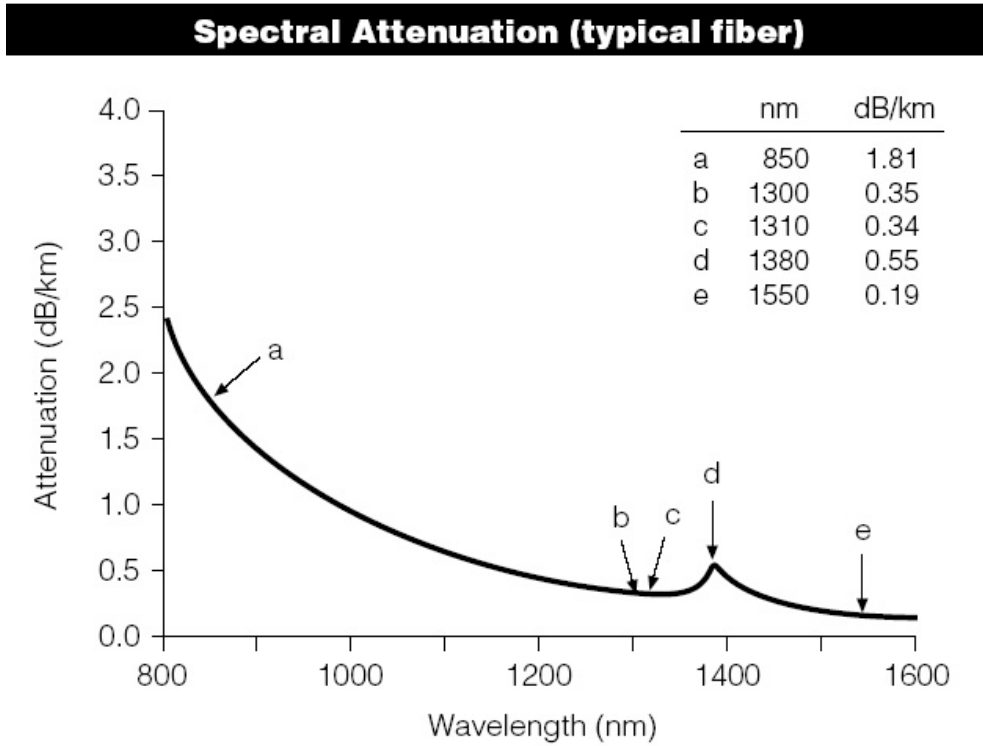


Figure 3. Spectral attenuation in a fused silica fiber [4]

B. Phase response to temperature changes in fiber

Factors which can affect the phase of light propagating in a fiber include static pressure, acoustic wave pressure, strain, and thermal fluctuations. Thermal variations can have a major effect on the phase of the light signal and must be accounted for in the sensor design [5]. The phase, ϕ , and phase change, $\Delta\phi$, of an optical signal in a fiber of length L are represented in (3) and (4) as

$$\phi = \frac{2\pi nL}{\lambda}, \quad (3)$$

$$\Delta\phi = \frac{2\pi\Delta(nL)}{\lambda}, \quad (4)$$

where n is the effective refractive index of the fiber mode and λ is the free-space wavelength of light. The effect of a temperature change, ΔT , on nL is given by

$$\Delta(nL) = \left(n \frac{\partial L}{\partial T} + L \frac{\partial n}{\partial T} \right) \Delta T. \quad (5)$$

The sensitivity to temperature is a major concern if looking at the phase effects in long stretches of fiber. For a silica fiber which has a very low thermal expansion coefficient, the effect of refractive index change is dominant - over 10 times greater than the effect of length change. To minimize thermal fluctuations it is imperative that a considerable effort to insulate the interferometers against temperature changes be undertaken to ensure accurate frequency drift data.

C. Phase shifts in a buried fiber

The sensitivity of a buried fiber optic cable to the pressure of an intruder crossing over it is a key issue in achieving a practical intrusion detection system. Even though it is possible to calculate the phase shift due to lateral pressure on a fiber, such calculations do not adequately account for the influence of the cable itself and the surrounding soil composition and conditions. Thus, in previous work, experiments were undertaken at Texas A&M to measure the phase change produced by a weight on the ground above a buried fiber cable.

In one series of experiments, the phase shift induced by pressure on a fiber cable buried in a sand box was investigated. The buried cable was spliced into one arm of an all-fiber Mach-Zehnder interferometer, and the phase shift was determined by

monitoring the pressure-induced phase fluctuations. A box with dimensions 30 cm x 10 cm (approximately the size of a human foot) was placed directly above the buried cable, and weights were added to the box to produce a π -radian phase shift as determined by monitoring the interferometer output power. For a depth of 20 cm a 60-kg intruder produced a phase change of about 6π radians, while for a 40 cm depth the phase change was about 2.5π radians. As expected, for a given burial depth the induced phase change was found to be close to a linear function of the applied weight [6].

Further investigations were made to determine if it was possible to avoid detection by stepping over the sensor cable. Fiber cable was buried at a depth of 30 cm in clay soil and it was found that a 60 kg intruder produces a π -radian phase shift within 2 meters on either side of the cable location.

D. Rayleigh scattering in optical fibers

The phenomenon of Rayleigh scattering accounts for nearly all (~96%) of the attenuation in today's fibers [7]. As light passes through the fiber it is scattered by random microscopic variations in the refractive index formed during the fiber drawing process, as in Figure 4. The light scatters in all directions, but a small fraction of the scattered light propagates in the reverse direction and is guided in the fiber core.

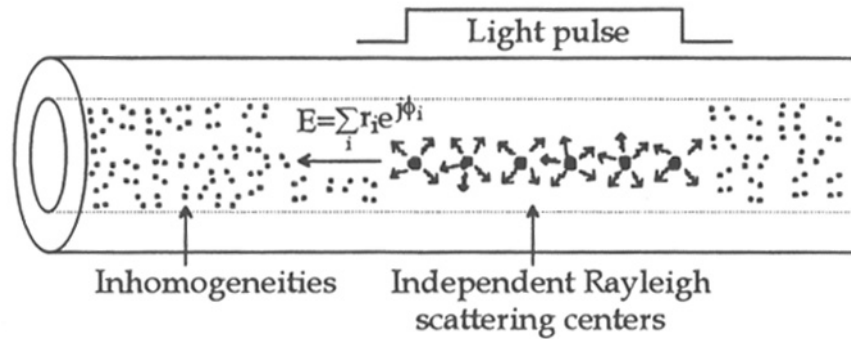


Figure 4. Rayleigh scatter in optical fiber [2]

The light that is backscattered towards the light source can be used in optical time domain reflectometry to monitor attenuation throughout the fiber length. Rayleigh loss decreases by $1/\lambda^4$ with increasing wavelength throughout the visible and near-infrared spectral regions, to about 1550 nm wavelength, beyond which the attenuation increases rapidly due to optical absorption resulting from the excitation of phonons in the fiber material. The minimum fiber loss at any wavelength is about 0.2 dB/km for 1550 nm light.

E. Mach Zehnder interferometer design

Interferometers are used for making measurements by determining relative phase shifts in optical path lengths. For this project, an unbalanced Mach Zehnder interferometer (MZI) was chosen. The MZI splits an input light beam into two different optical paths, and then recombines the two beams after traveling their two

separate path lengths. In the case of the unbalanced MZI one path is lengthened as in Figure 5, adding a delay component to the interference.

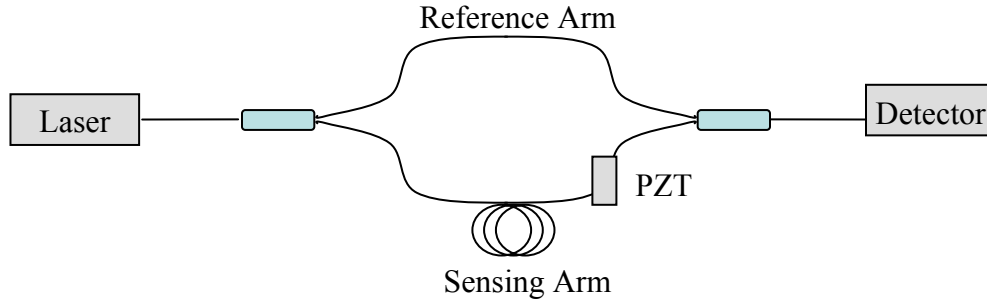


Figure 5. Unbalanced Mach Zehnder

The detected output waveform represents the interference of light emitted by the laser at time t with light emitted at time $t + \tau$, with τ given by

$$\tau = \frac{n_g \Delta L}{c}, \quad (6)$$

with n_g the group refractive index of the fiber mode, ΔL the fiber length difference in the interferometer, and c the free-space speed of light. Thus, with $n_g = 1.46$, $\Delta L = 200$ m (as in the present work) and $c = 3 \times 10^8$ m/sec,

$$\tau = \frac{1.46 * 200}{3 * 10^8} = 0.97 \mu\text{sec}. \quad (7)$$

The interferometer output signal indicates the rate of frequency drift in the laser, with one complete period (fringe) - indicative of a 2π radian relative phase shift - corresponding to a frequency change of $1/\tau$. In the present case, one fringe represents a

laser frequency drift of 1.03 MHz. The photodetector signal received at the output coupler of the MZIs is digitized by a data acquisition card and stored in the memory of a personal computer. Once in the computer, the drift rate data can be analyzed and plotted.

F. Laser linewidth

The linewidth or spectral width of the laser light is an intrinsic property that can affect the ability to utilize the coherence of the laser light [8]. The difference between the ϕ -OTDR and the conventional OTDR is in the light source linewidth. The conventional OTDR uses a current-modulated laser diode with a spectral width $\gg 1/\tau$, with τ the laser pulse width. Thus, if $\tau = 1$ nsec, corresponding to 10 cm spatial resolution, then the spectral width of the laser pulses is $\gg 1$ GHz. (From a practical standpoint, since OTDRs generally use multimode Fabry-Perot lasers, the spectral width is in the hundreds of GHz range). The broad laser spectrum ensures a smooth OTDR trace which depends on the amplitude but not relative phases of the waves which contribute to the Rayleigh-backscattered light. On the other hand, the ϕ -OTDR requires a light source spectral width $\ll 1/\tau$ so that phase changes along the fiber will strongly affect the observed response. As an example, if $\tau = 1$ μ sec, corresponding to a 100 m spatial resolution, then the spectral width should ideally be $\ll 1$ MHz.

G. Frequency drift in lasers

The availability of a laser with narrow instantaneous linewidth and very low frequency drift is the key to a successful demonstration of the intrusion sensor. As mentioned above, if the instantaneous spectral width of the laser is $\gg 1/\tau$, with τ the width of the laser pulse, coherent effects will disappear and a smooth OTDR trace which is insensitive to phase changes will be observed. Even if the instantaneous spectral width is $\ll 1/\tau$, the laser will still not be satisfactory if its frequency drifts significantly as the intrusion-induced pressure change is occurring. Suppose, for example, that a slow-moving intruder produces a phase perturbation in light propagating in the fiber which goes from 0 to π -radian in 1 second. A frequency drift in the laser of $1/\tau$ which occurs during 1 sec will produce optical power changes in each time bin on the order of the change which would result from this intruder-induced phase shift. For that reason, it is important that the frequency drift be $\ll 1/\tau$ over the time frame during which a dynamic change occurs. Thus, in the present example with $\tau = 1 \mu\text{sec}$ and the perturbation occurring over a one second time interval, the laser frequency drift rate should be much less than 1 MHz/sec.

H. Erbium doped fiber amplifiers

With the increased use of optical fiber throughout the world came the need to boost the signal over long stretches of fiber. Prior to the advent of optical amplifiers the only way to boost signal levels in fiber optic communication systems were optical

to electrical to optical (OEO) conversion through the use of optoelectronic repeaters [9]. However, each optoelectronic repeater was expensive and one was required for each wavelength-division-multiplexed (WDM) channel in an optical communication system. Various optical amplifier technologies have been developed, including semiconductor optical amplifiers, rare-earth-doped, fiber amplifiers, and Brillouin and Raman amplifiers, each of which has its own advantages and disadvantages [10]. Of all the candidates, the erbium doped fiber amplifier (EDFA) has emerged as the technology of choice for optical telecommunication.

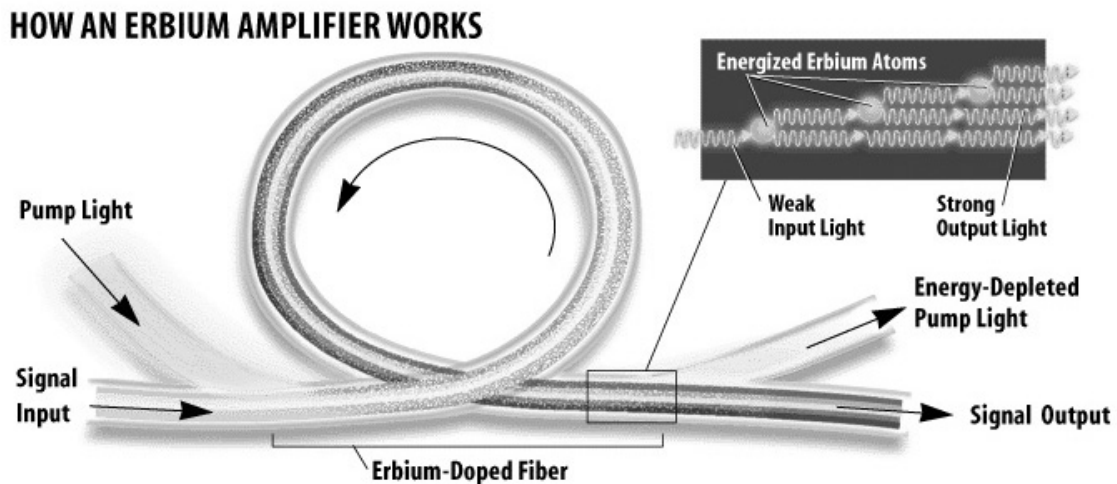


Figure 6. Operation of EDFA [9]

The EDFA operates by injecting pump light into doped fiber to boost electrons in Er^{3+} atoms from the ground state to an excited state, as in Figure 6. Erbium ions (Er^{3+}) have a lasing transition at $1.5 \mu\text{m}$, which happens to coincide with the spectral region of lowest loss in a silica fiber. Furthermore the two strongest absorption bands in

erbium correspond to wavelengths of 980 nm and 1480 nm; wavelengths at which semiconductor laser pump diodes can be fabricated with sizeable output powers [11]. EDFAs, which can simultaneously boost signal levels in many WDM channels in a single fiber, are widely used for signal regeneration in optical fiber communication systems.

I. OTDR configuration

The optical time domain reflectometer (OTDR), initially demonstrated over two decades ago [12-14], is now widely used for locating breaks and other anomalies in fiber optic links and networks. In such a system, light pulses from a semiconductor laser are injected into one end of a fiber, and the light returned from the fiber by Rayleigh backscattering is monitored with a photodetector, as in Figure. 7. The OTDR detects the presence and location of perturbations which affect the intensity of the light returned from the fiber, but does not in general respond to phase modulation of the light. The spectral width of the modulated laser is very broad (GHz to THz range), so that fluctuations in the return signal due to interference of backscattered components from different parts of the fiber are avoided. When present to a noticeable extent, coherent effects represent an undesirable source of noise in an OTDR trace [15].

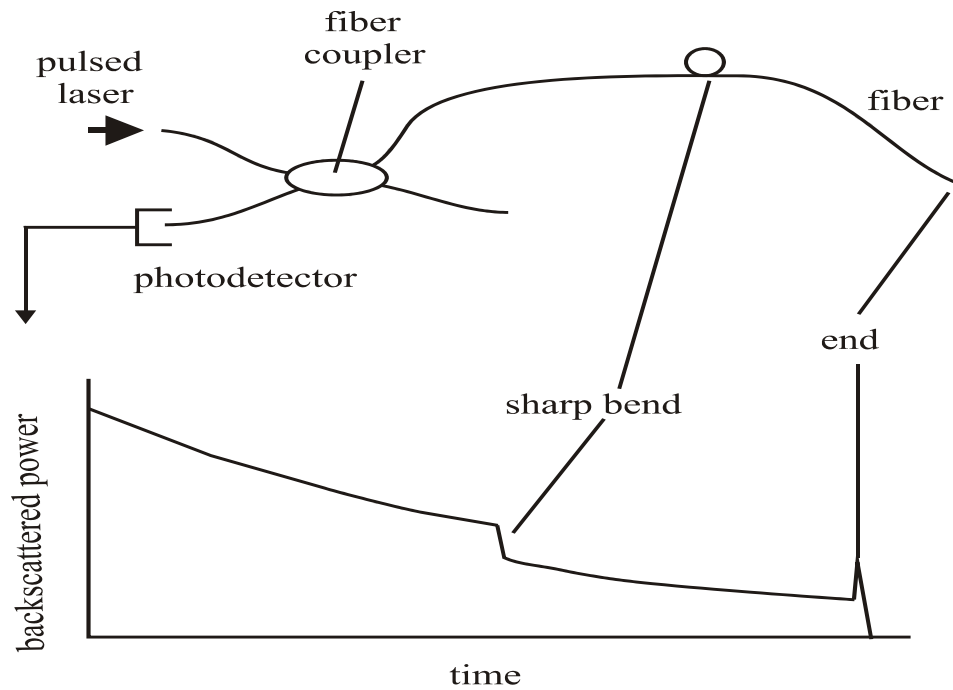


Figure 7. Optical time-domain reflectometer (OTDR)

J. Configuration for ϕ -OTDR intrusion sensor

In the perimeter security sensor investigated here, phase changes resulting from either the pressure of the intruder on the ground immediately above the buried fiber or from seismic disturbances in the vicinity are sensed by a phase-sensitive optical time-domain reflectometer (ϕ -OTDR) [15,16]. The sensitivity of conventional OTDRs to small perturbations is orders of magnitude too low for this application because of the broad spectrum of the light source. For the ϕ -OTDR, light pulses from a continuous wave laser with a narrow (kHz-range) spectral width are gated into one end of the fiber via a pulsed intensity modulator, and the backscattered light from the fiber is

monitored with a photodetector. As with the conventional OTDR, the ϕ -OTDR trace is a plot of returned optical power vs. time. Phase sensitivity results from coherent addition of amplitudes of the light backscattered from different parts of the fiber which arrive simultaneously at the photodetector. In contrast to the conventional OTDR, the ϕ -OTDR requires a laser with minimal frequency drift as well as narrow instantaneous linewidth. The Er: fiber laser is an attractive candidate because it emits in the spectral region where silica fiber losses are at a minimum, it can be used with Er: fiber amplifiers to achieve high average and pulsed power levels, and it can be configured to emit in a single longitudinal mode for narrow linewidth operation.

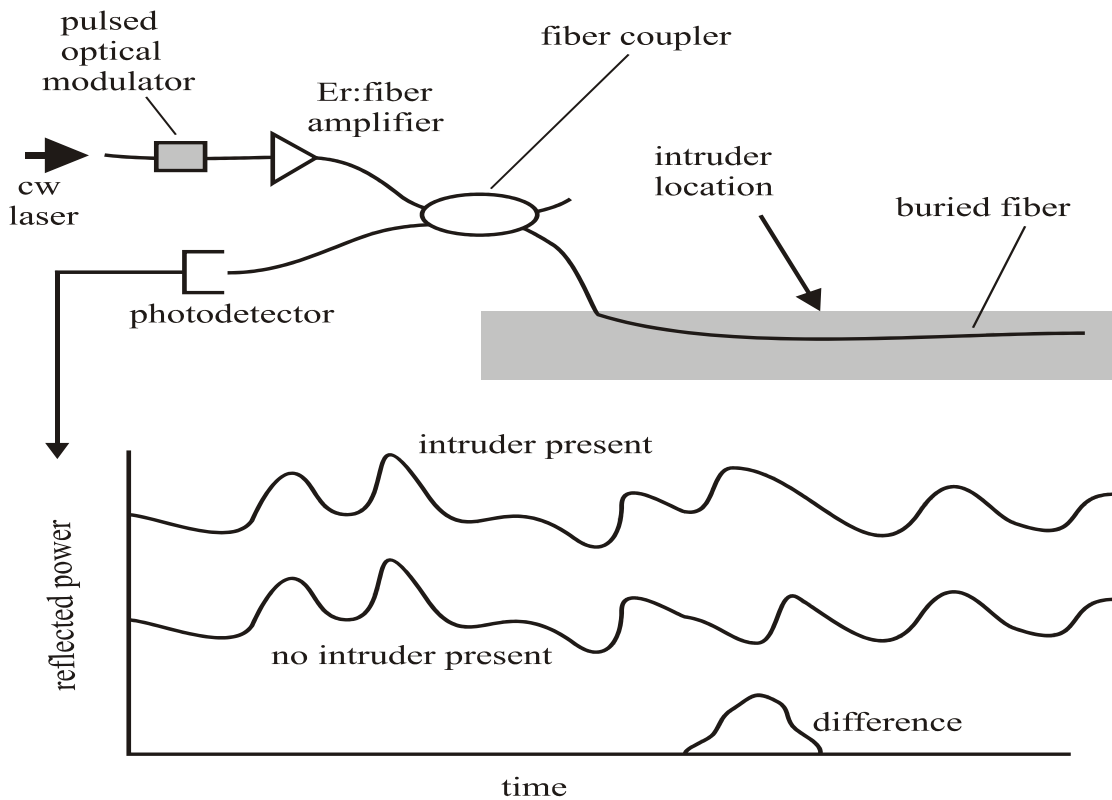


Figure 8. Configuration for ϕ -OTDR intrusion sensor [16]

The ϕ -OTDR intrusion sensor is illustrated schematically in Figure 8. Light from the frequency-stabilized Er:fiber laser passes through an integrated optical modulator, which gates an optical pulse through a 3-dB coupler and into a multi-kilometer stretch of buried fiber optic cable. Rayleigh backscattered light passes through the coupler and is collected by a photodetector. If the laser emits a single optical frequency which does not change with time, and no optical phase changes occur over the fiber length, the ϕ -OTDR traces will be the same from one laser pulse to the next. However, when an intruder causes a phase shift to occur, the trace will be affected at a time corresponding to the location of the intrusion. By subtracting the most recent trace from a previous stored trace, the intruder can be detected and located.

When a short light pulse is coupled into the fiber, the duration T of the return pulse will be given by

$$T = \frac{2Ln_g}{c}, \quad (8)$$

with L the length of the fiber, n_g the refractive index of the fiber and c the free space speed of light. For a silica fiber with $n_g=1.46$, it is calculated that $T= 9.73L$ with T in μs and L in km. Thus, for a 12 km path length, the duration of the return signal is $117\mu\text{s}$. With a simulated disturbance at the 2 km point the phase shift would be detected $20 \mu\text{s}$ into the trace.

Previous theoretical calculations on such a ϕ -OTDR intrusion sensor conducted by Texas A&M [16] predicts a dependence of range resolution on detection range for such a sensor given by Figure 9.

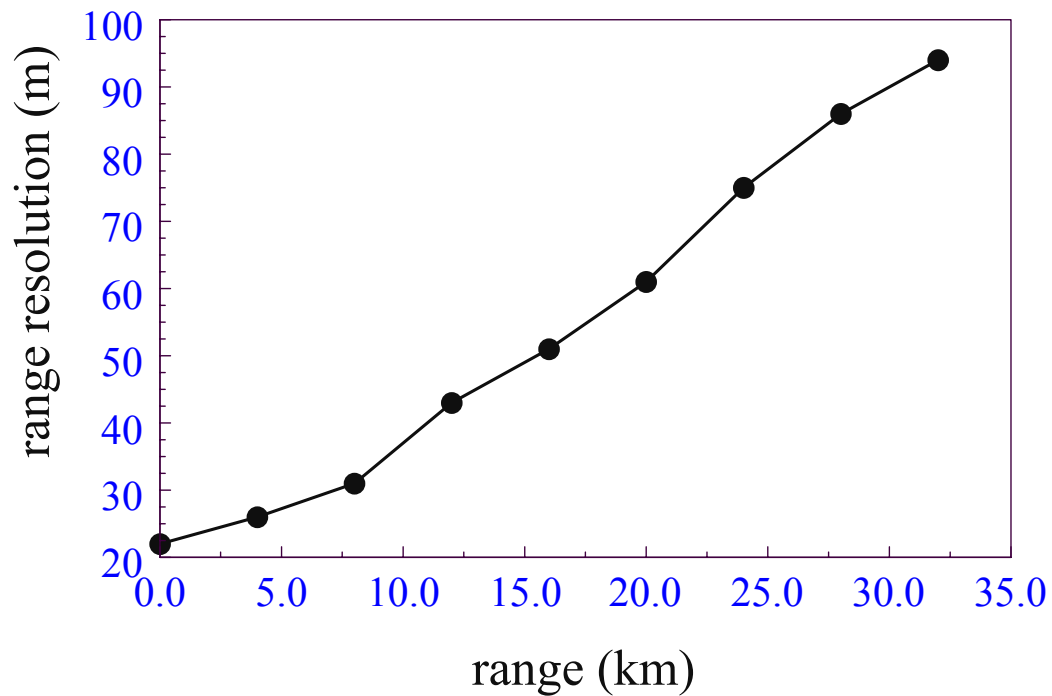


Figure 9. Simulated dependence of range resolution on range in fiber [16]

For perimeters as large as 35 km the theoretical analysis suggest resolution of intrusion points as small as 100 m. Factors such as environmental conditions will have an effect on such calculations, but with sufficient insulation this sensor system will have monitoring capabilities that far surpass many of today's resolution standards for long-range perimeters.

CHAPTER III

EXPERIMENTAL PROCEDURES

A. Laser stabilization

For the operation of the fiber intrusion sensor, a highly stable light source is needed for transmission throughout the perimeter of buried fiber to achieve accurate measurement. In previous work in the Electrical Engineering Department at Texas A&M, a narrow line, low-drift rate erbium-doped fiber laser (EDFL), Figure 10, was developed [15] and applied to the first laboratory demonstration of the ϕ -OTDR [16]. However, substantial improvements in the laser drift rate and a reduced sensitivity to vibration and acoustic effects were needed before field tests could be carried out.

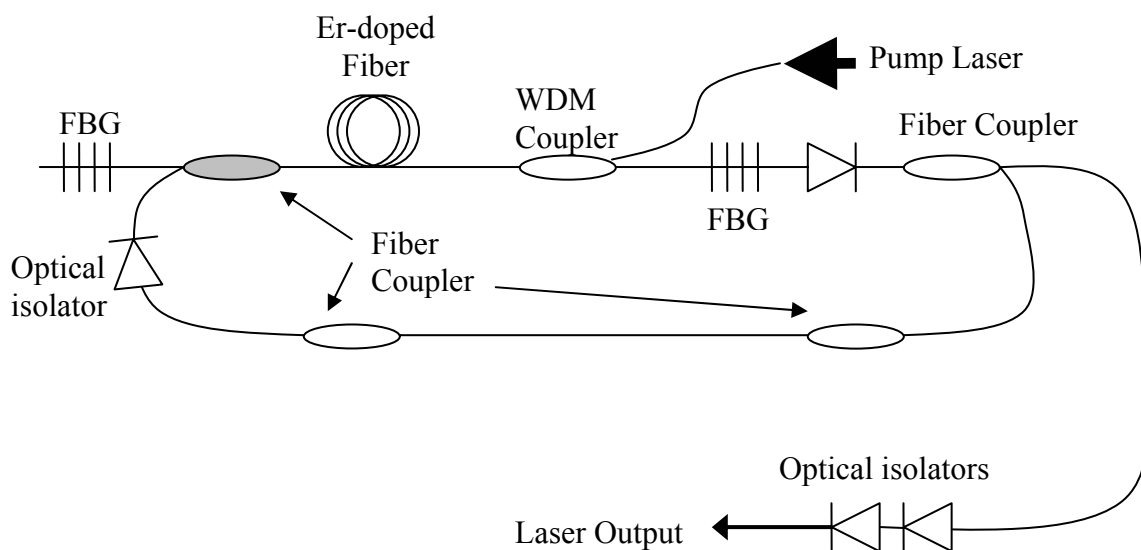


Figure 10. EDFL design

The EDFL is comprised of a Fabry-Perot cavity formed by two fiber Bragg grating (FBG) reflectors with identical reflectance peak wavelengths of 1555.6 nm and spectral widths of 0.4 nm. The three meter long Er^{+3} doped fiber gain medium is pumped by a 980 nm semiconductor laser. Optical feedback paths are added to improve the spectral characteristics of the laser – a short (2 m) path to reduce the instantaneous linewidth and an optional long (25 km) path with an in-line Er: fiber optical amplifier with a small signal gain of 20 dB to suppress the frequency drift. Sufficient stabilization effects were not seen with the long feedback path in this experiment, so only the short path was used for these measurements. Optical isolators ensure unidirectional propagation in the feedback loop and suppress coupling of the laser emission back into the cavity. The spectrum of the laser, showing a linewidth limited by the 0.05 nm resolution of the spectrum analyzer, is shown in Figure 11.

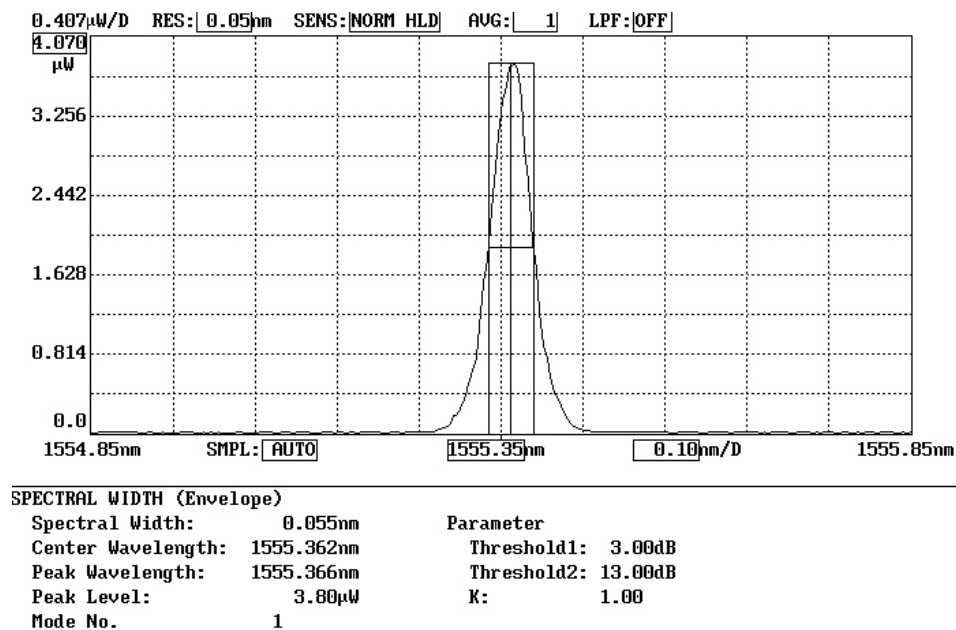


Figure 11. Spectral linewidth scan of EDFL

To achieve ultra-stable operation, the laser cavity and feedback loops are housed in a thermally insulated enclosure (Figure 12a), as a constant temperature environment is essential to achieving a stable lasing spectrum. Similarly the MZIs were housed in thermally stable environments to protect against disturbances. The enclosures were built of Styrofoam panels and lined with insulation with a high R value for thermal stabilization.



Figure 12. A) Laser and feedback path housing B) MZI housing

The MZI enclosure is actually two boxes in one with the smaller inner box as seen above lined with foam and then placed in a larger box surrounded by insulating materials. The laser and MZIs were enclosed and sealed to suppress acoustic and

thermal effects. To eliminate internal heat generation the pump laser and its power supply are located outside of the insulated enclosure containing the EDFL.

B. Mach Zehnder fabrication

To characterize the frequency drift of the laser, two identical all-fiber Mach Zehnder interferometers (MZIs) will be used. As illustrated in Figure 5, the MZIs are designed with one long optical path and one short one, so that the relative phase difference $\phi_1 - \phi_2$ in the interferometer is given by

$$\phi_1 - \phi_2 = \frac{2\pi n \nu}{c} (L_1 - L_2), \quad (9)$$

with n the effective refractive index fiber mode, ν the laser frequency, L_1 and L_2 the lengths of the fiber arms, and c the free-space speed of light. If the laser frequency drift is linear with time, the relative phase shift can be written

$$\phi_1 - \phi_2 = \frac{2\pi n}{c} (L_1 - L_2) (\nu_0 + \alpha t), \quad (10)$$

with α the frequency drift rate. The photodetector signal current I can be written

$$I = I_0 [C_1 + C_2 \cos(\phi_1 - \phi_2)], \quad (11)$$

with I_0 , C_1 , and C_2 constants. If the laser frequency drift is linear in time as in (10), the photodetector signal will vary sinusoidally, sweeping through interference “fringes” at a rate proportional to the frequency drift rate.

A piezoelectric cylinder (PZT) with fiber wrapped around it is deployed in one arm of the interferometer as shown in Figure 13. When a voltage is applied to the PZT,

the fiber is stretched to produce a phase shift. Applying periodic voltage pulses to the PZT provides a time reference and also verifies the “fringe visibility” of the MZI.

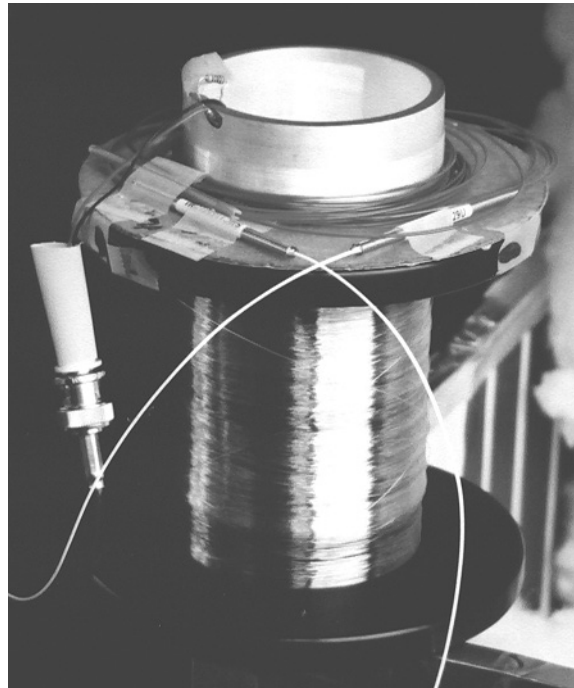


Figure 13. Mach Zehnder interferometers

C. Frequency drift set up

Once the preceding components are stabilized it is possible to monitor the frequency drift of the laser as in Figure 14. By housing the two interferometers separately in heavily insulated boxes (Figure 12b), two independent measurements of the laser frequency drift can be made simultaneously. The laser output power is first boosted by a fiber amplifier, and then passes through a 3-dB coupler to split the light equally into the two paths. Each coupler output is then connected to the input of one of

the Mach Zehnder interferometers. To verify the operation and provide the time reference the PZTs are connected to a pulse generator producing a low frequency pulse. The pulse generator produces peaks with a max voltage of 5 volts so an amplifier circuit (Appendix B) was designed to amplify to approximately 12 volts to verify the 2π shift. The interferometer data is acquired with photodetectors and input to a LabView data acquisition system, stored in a personal computer memory, and plotted.

The drift rate recorded by each photodetector represents the combined effects of the laser and one of the Mach Zehnders. By utilizing two Mach Zehnders and verifying similar readings, an accurate drift rate can be ascertained. The interferometer data is also useful in assessing “mode hopping” (sudden frequency shifts) in the laser, which results in discontinuous changes in the MZI fringe patterns.

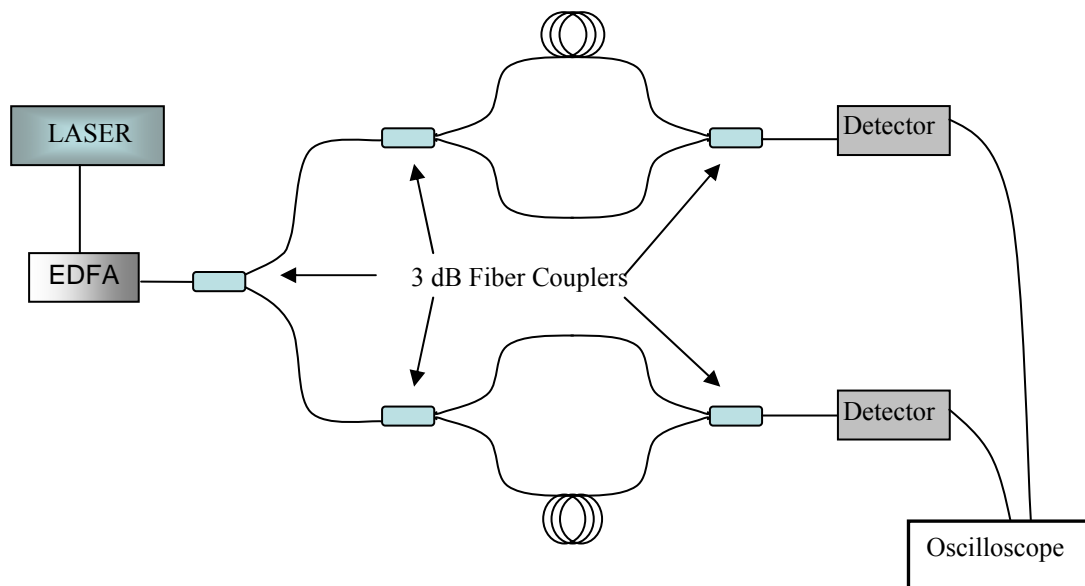


Figure 14. Frequency drift experimental set up

D. ϕ -OTDR set up

After the laser frequency stability was verified, the performance of the ϕ -OTDR was investigated using the arrangement of Figure 15. The light from the stable EDFL is first sent through a bandpass filter to remove unwanted spontaneous emission. The light is then sent through an optical amplifier to boost the signal at which point an electro-optic (EO) modulator is used to gate light pulses a few μsec wide into the sensing fiber. However before the light enters the sensor path length the optical power in the pulse is increased by 20 – 30 dB by an erbium-doped fiber amplifier (EDFA). The light then passes into the sensing fiber through a 3 dB fiber coupler, and the return light is monitored with a photodetector. A phase change is introduced using a piezoelectric transducer (PZT) to produce longitudinal strain in the fiber at a distance of 2 km from the input end. The optical return signal from the fiber is converted to an electrical signal and observed using an oscilloscope.

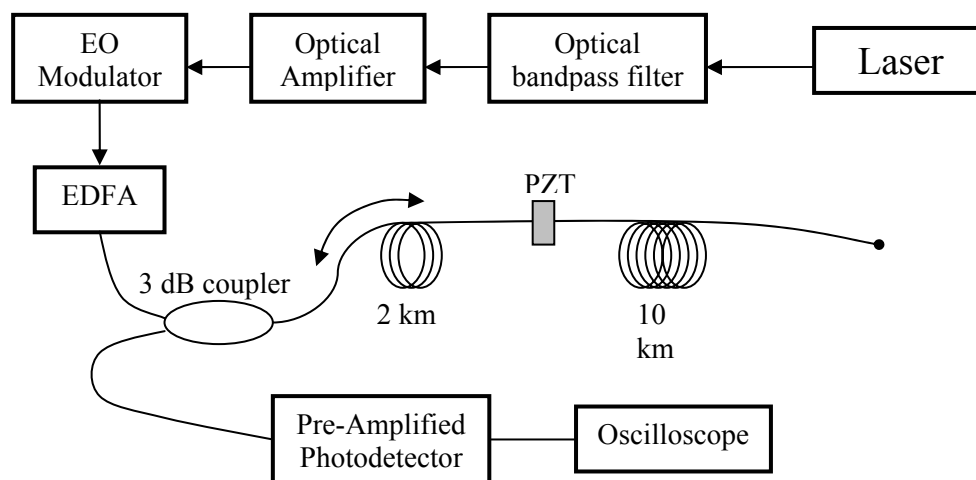


Figure 15. ϕ -OTDR experimental set up

As the PZT is pulsed a distinguishable variation is observed in the ϕ -OTDR traces. By comparing a control trace with no PZT modulation to a trace obtained when the PZT voltage is applied, the phase disturbance can be both detected and localized. Averaging of the oscilloscope traces over multiple pulses of the laser will improve the signal to noise ratio of the ϕ -OTDR data and give information on the effect of laser frequency drift.

CHAPTER IV

RESULTS

A. Frequency drift results

Using the experimental arrangement described in Chapter III the frequency drift of the EDFL was monitored with the two Mach Zehnder interferometers. The tests were performed in a temperature controlled laboratory setting on a vibration-isolated optical table. The set up was connected as in Figure 14 with the laser light coupled into the two MZIs after amplification by the EDFA and splitting with a 3 dB coupler. The output of each individual MZI was then converted to an electrical signal with a photodetector. MZI A's signal, boosted using a low noise electronic amplifier, served as an analog input to the data acquisition card. MZI B's photodetector output, with a 10 k Ω resistor in parallel, was the second input to the data acquisition card. The data was logged using a LabView program and presented in Excel spread sheet format to generate a graphical representation of the temporal dependence of the interferometer output signals as an indication of the frequency drift. The first attempts to characterize the drift rates, conducted with the Mach Zehnders in an open-air environment on the optical table, revealed a very unstable drift rate as the MZIs were subject to acoustic effects and temperature fluctuations.

At this point stabilized enclosures were designed and constructed in an attempt to decrease the effects of the environment. Initially one MZI was secured in the new

housing and the other was left exposed on the optical table to compare the effects of the enclosures. The thermally and acoustically isolated housing made a vast difference in the fringe rate observed in the interferometers as shown in Figure 16. This gave the first true indication that the initial heightened fringe rate was not an effect of the laser but rather the Mach Zehnders themselves. Based on these findings further effort went into stabilizing the enclosures to obtain a more accurate characterization of the frequency drift. Once completed, the boxes were placed on the optical table to reduce

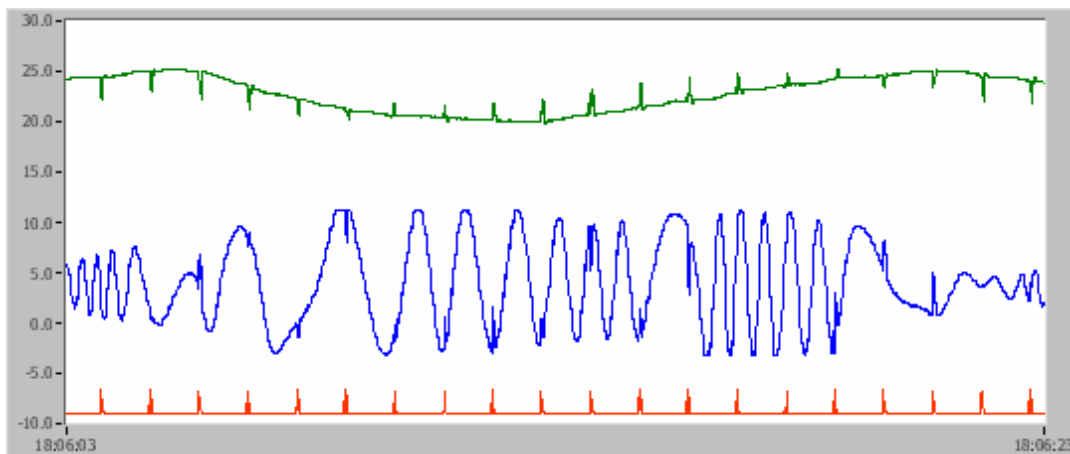


Figure 16. Frequency drift comparison of enclosed MZI vs. open (top signal in enclosed box, bottom in open air) over 20 seconds. The pulses in the fringe curves result from square-wave voltage pulses applied to the PZTs (Fig. 14).

the effects of vibrational disturbances due to movement of people in the laboratory as well as disturbances outside the building. Based on observation however it could be seen that speech and even cars passing on the street (50 feet away) could still cause enough disturbance to send the light through a multiple π radian shift. For example,

when tapping on the table near the housings a large fringe disturbance could be seen (Figure 17).

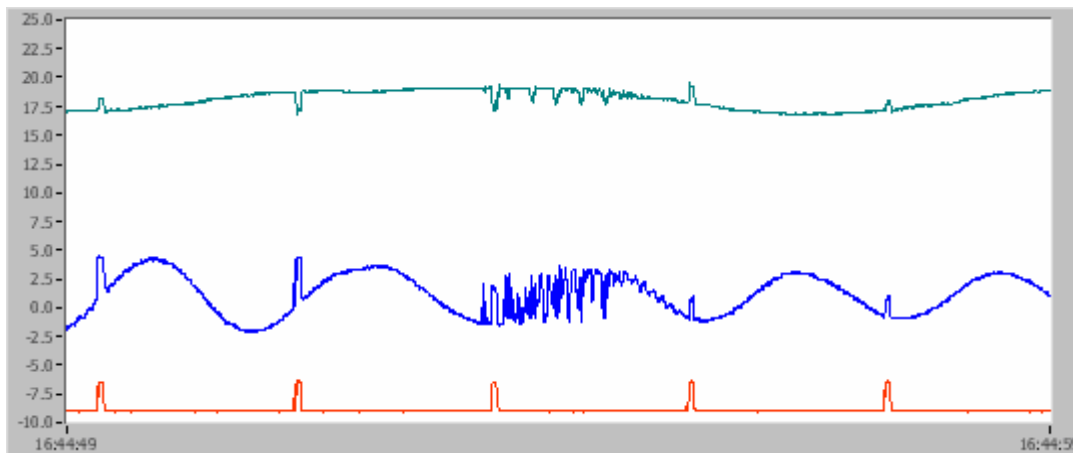


Figure 17. Phase disturbance experienced when tapping near the box (5 sec)

Based on these findings most of the further experimental work was conducted during the night to eliminate as much of the outside disturbances as possible. Figures 18 - 20 show the drift stabilization as the laser was monitored at 3 p.m., 10 p.m. and 3 a.m. respectively. As shown in the data, the effect of people in the building and automobile traffic outside was less at night than during the daytime, so the fringes became much more stable.

Longer traces were taken while the set up was left to run over the course of a weekend when disturbances were at a minimum. Figures 21 - 23 show three consecutive 5 minute drift readings taken at 6:12 a.m., 6:17 a.m., and 6:22 a.m. respectively. The frequency drift data taken overnight showed a drift rate of about 1 fringe per 14 minutes, or an average of $1000 \text{ kHz/fringe} \times 1 \text{ fringe}/14 \text{ min} \times 1 \text{ min}/60 \text{ sec} = 1.2 \text{ kHz/sec}$ - well below drift rates of about 1 fringe/minute seen previously.

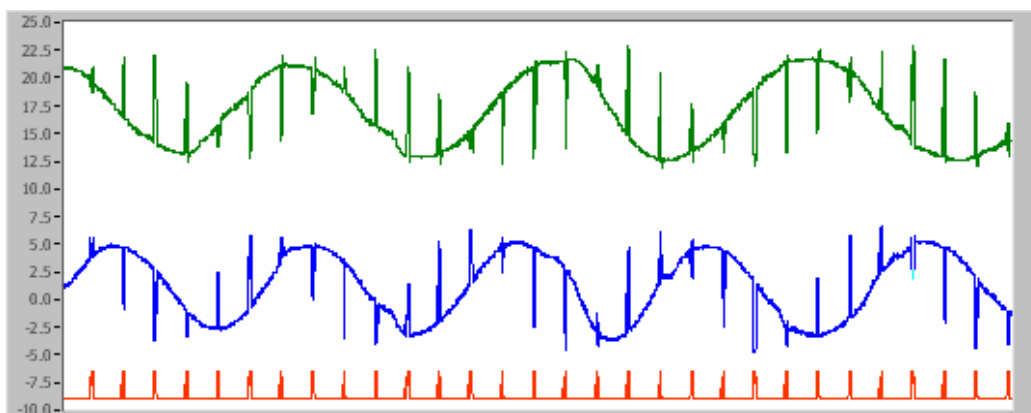


Figure 18. Frequency drift 3 p.m. (30 sec)

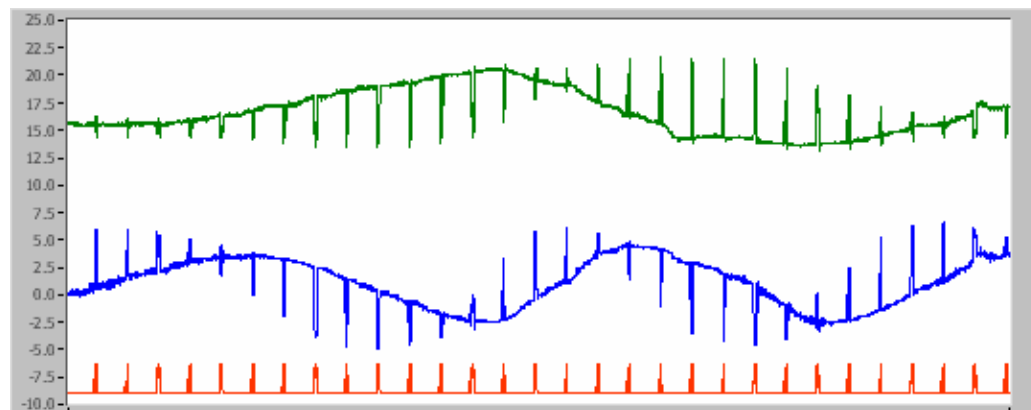


Figure 19. Frequency drift 10 p.m. (30 sec)

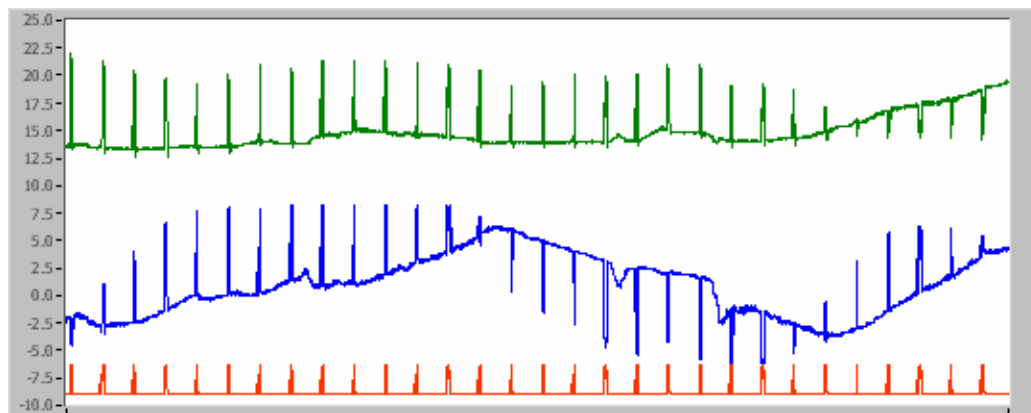


Figure 20. Frequency drift 3 a.m. (30 sec)

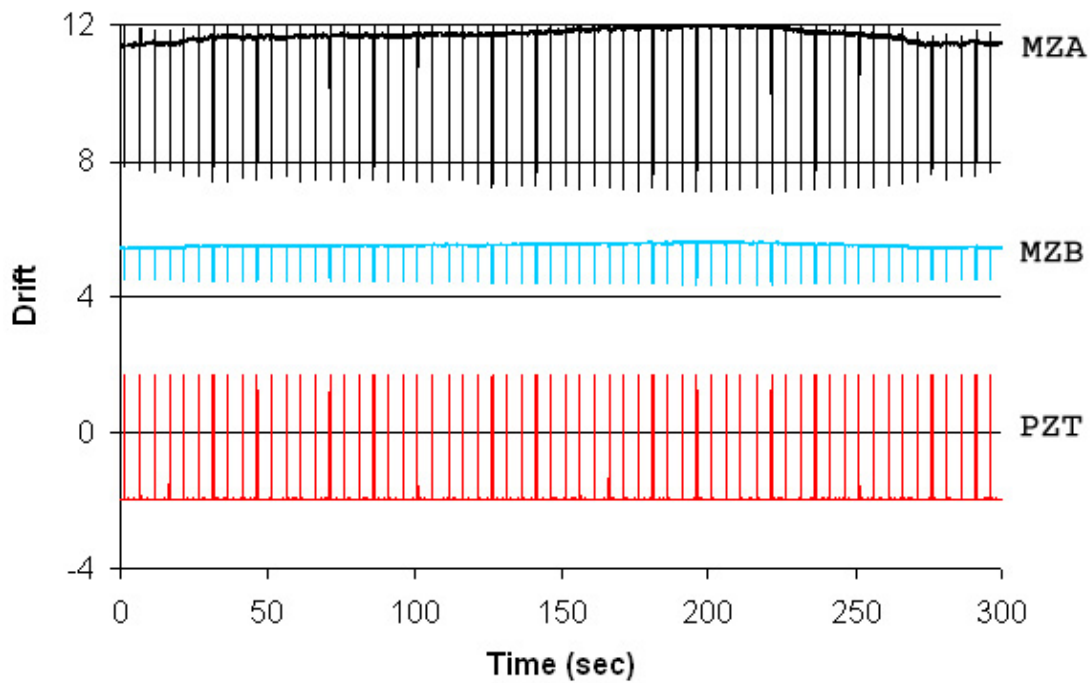


Figure 21. Frequency drift 6:12 a.m.

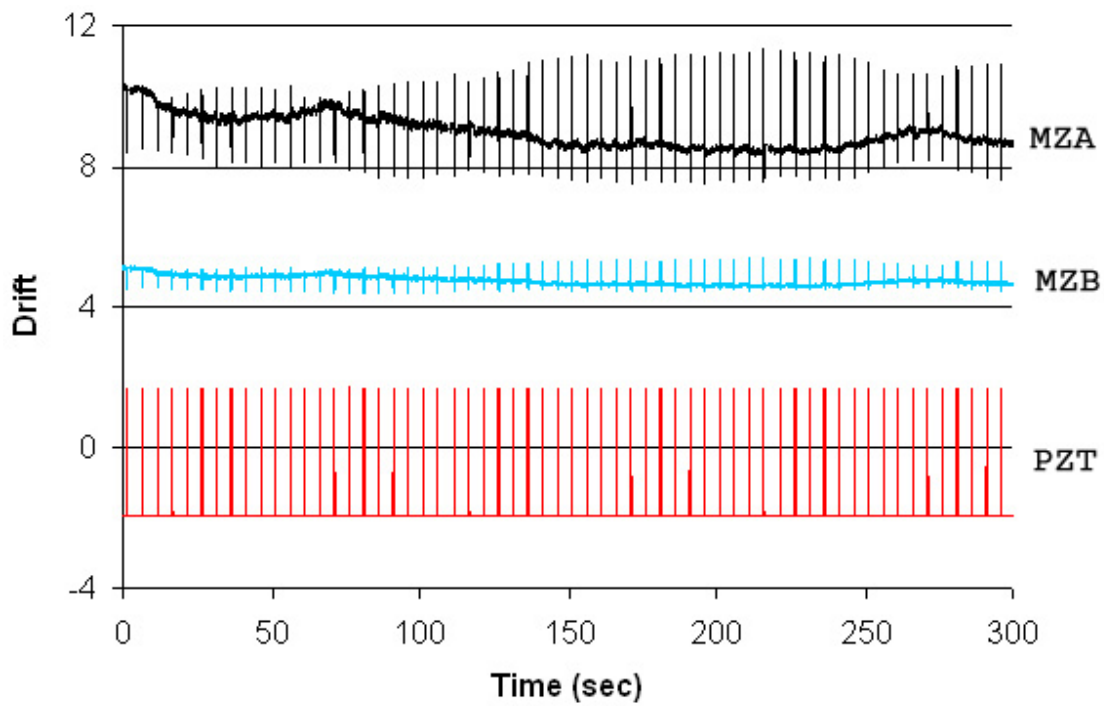


Figure 22. Frequency drift 6:17 a.m

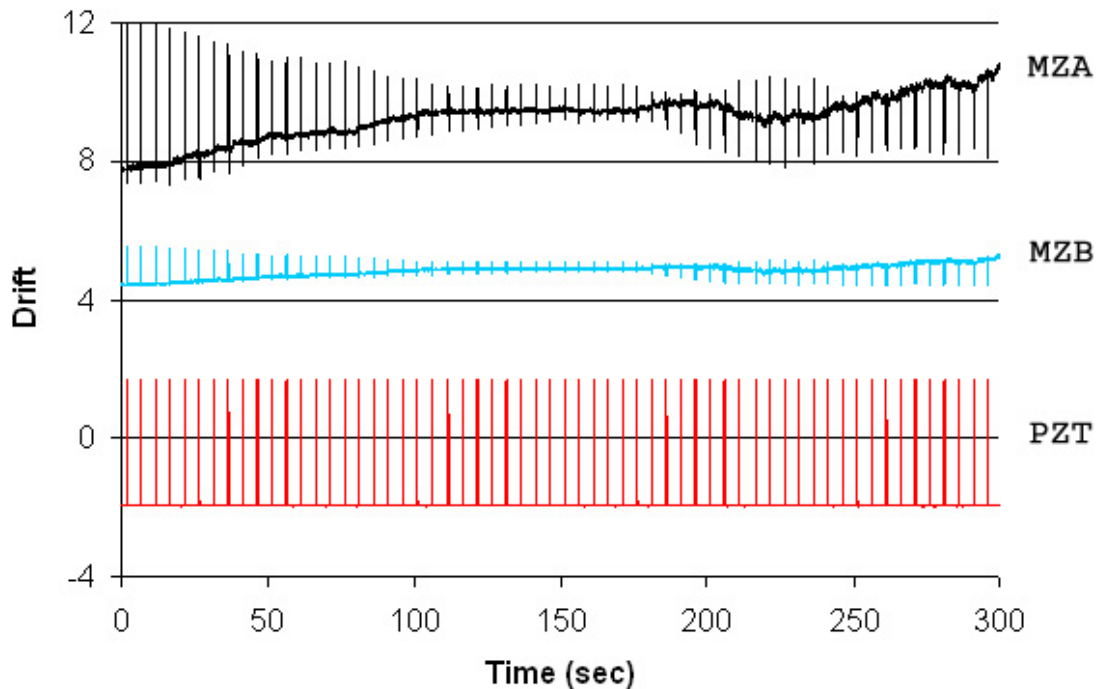


Figure 23. Frequency drift 6:22 a.m.

The PZT pulse delivered to the interferometers was generated using a pulse generator triggered by a function generator sending a low frequency square wave. The PZT pulse not only provided a time reference but also served to verify the operation of the interferometers. The pulse should create a 2π radian shift to verify that the phase disturbance takes the drift through a complete fringe. To show that this was indeed taking place the drift data was recorded as increasing voltages were placed on the PZT. Figures 24 – 31 show the effects of increasing the voltage supplied to the PZT and therefore the amount of displacement in the fiber. As can be seen in the later figures the data indeed goes through a complete 2π shift verifying the accuracy of the frequency drift data.

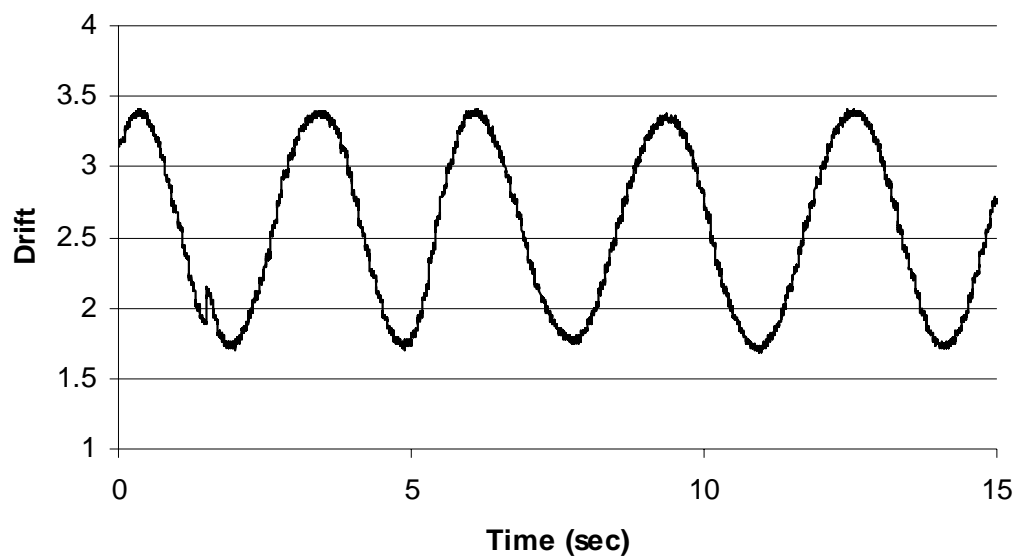


Figure 24. Drift rate with 0.0 Volts

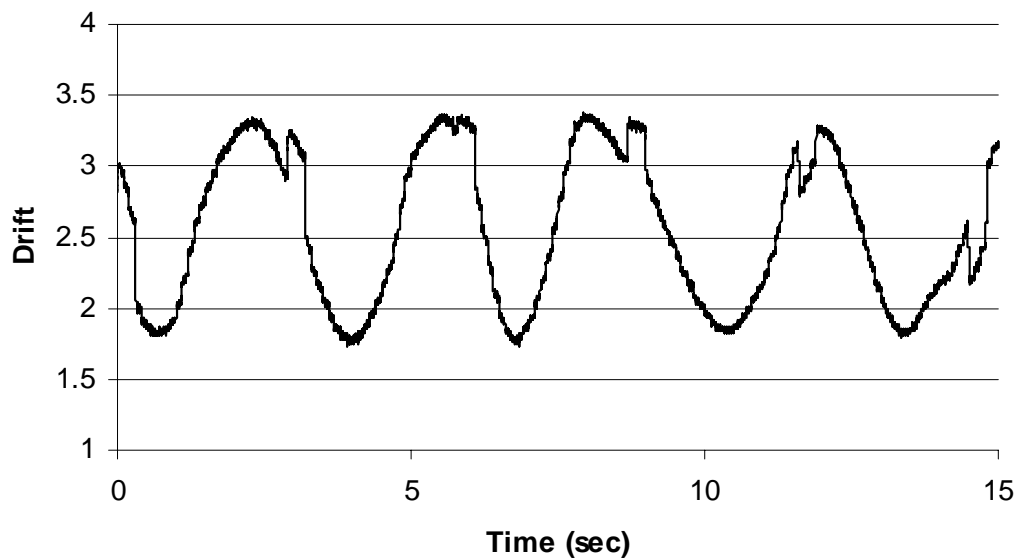


Figure 25. Drift rate with 0.5 Volts

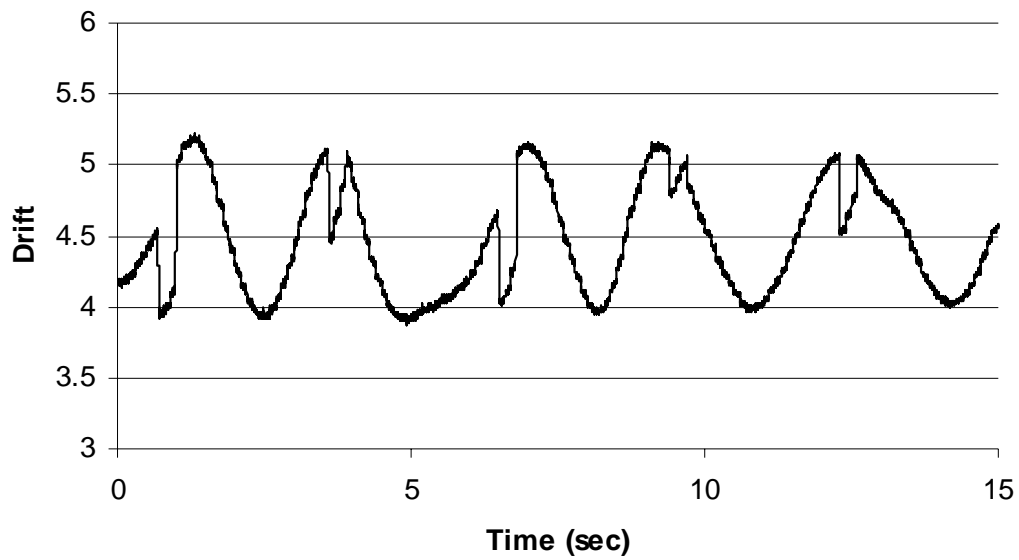


Figure 26. Drift rate with 1.0 Volts

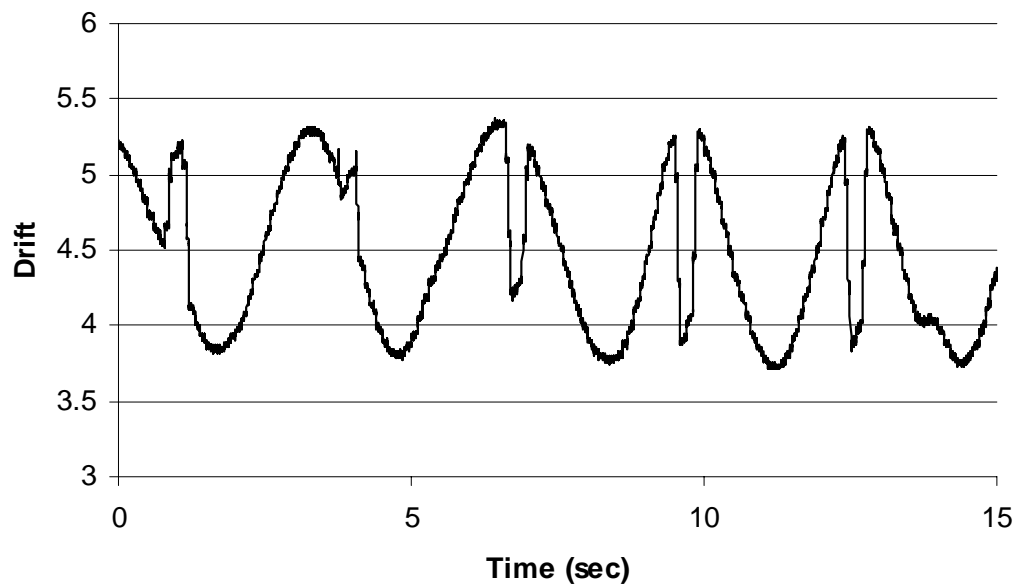


Figure 27. Drift rate with 1.5 Volts

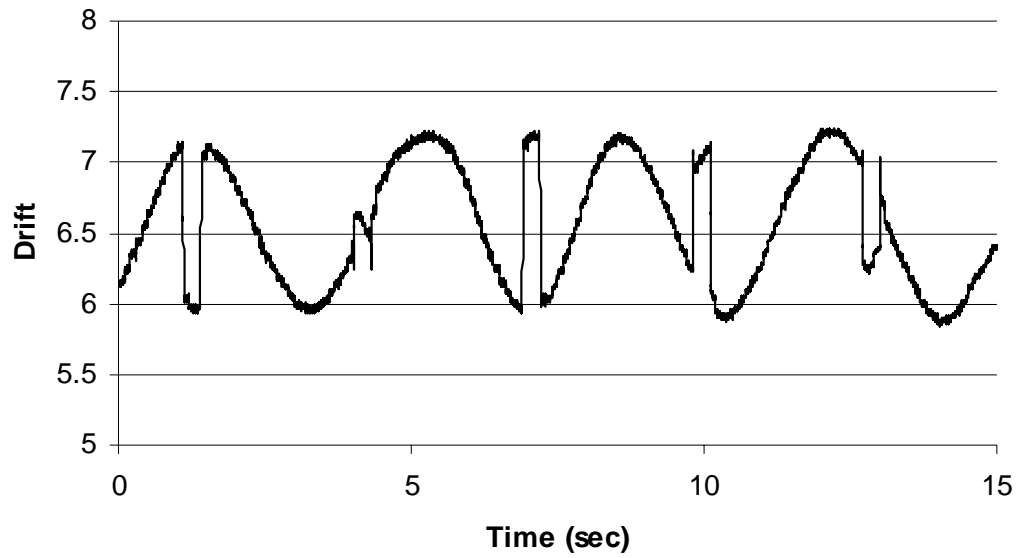


Figure 28. Drift rate with 2.0 Volts

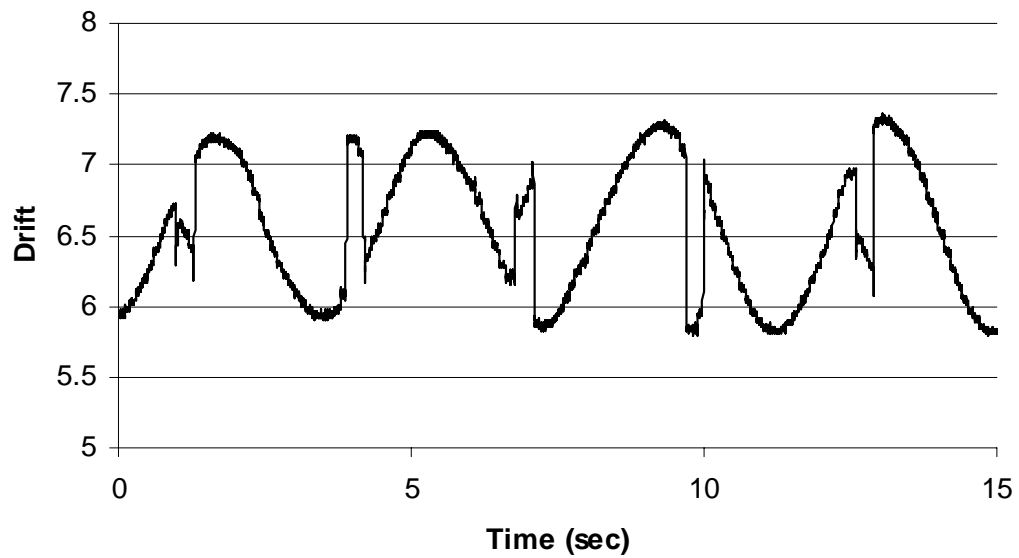


Figure 29. Drift rate with 2.5 Volts

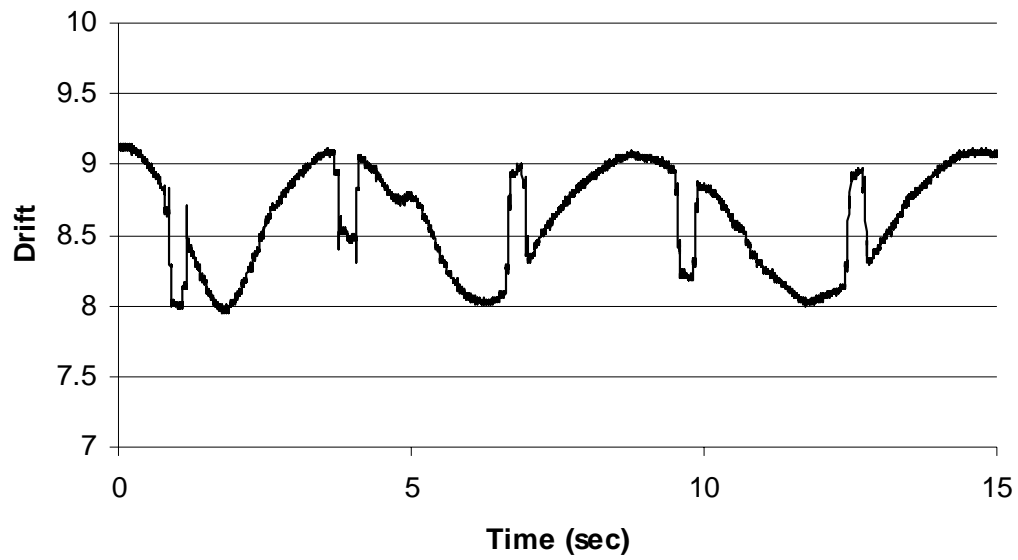


Figure 30. Drift rate with 3.0 Volts

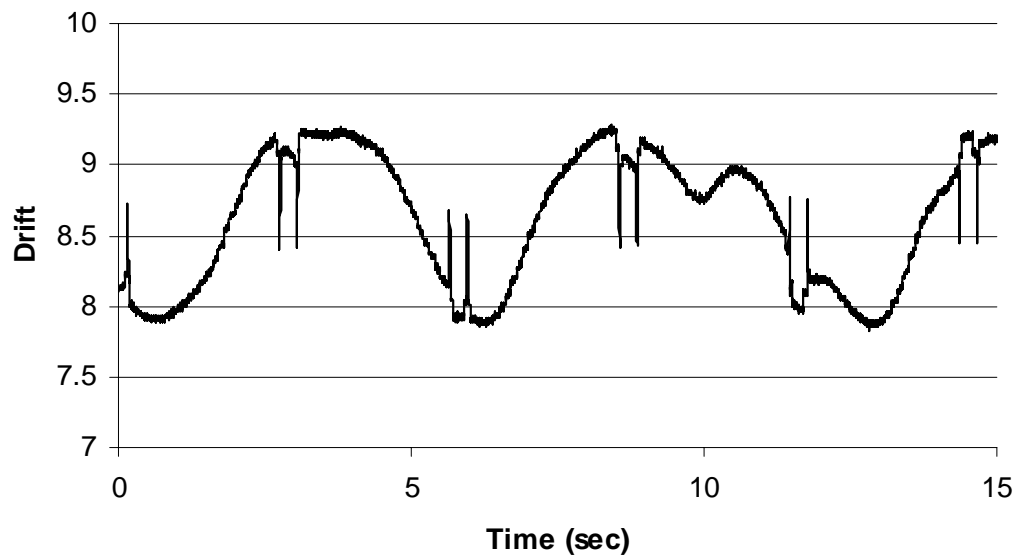


Figure 31. Drift rate with 3.5 Volts

B. Intrusion simulation results

Based on these results described above, the ϕ -OTDR experiment was undertaken with sufficient comfort in the level of stability of the laser. The setup shown in Figure 15 was constructed to determine the ability to detect disturbances in long stretches of fiber. The EDFL light was gated through an electro-optic modulator producing pulses every 150 μ sec. These pulses passed through an EDFA, a 3 dB coupler, and into a 12 km length of fiber. At the 2 km point of this sensing fiber a PZT was inserted to simulate the “intrusion” by introducing an “impulse” phase shift. The other coupler leg was connected to a photodetector, the signal from which was amplified and displayed on an oscilloscope.

The initial step was to acquire a stable ϕ -OTDR trace on the oscilloscope. Early attempts to acquire a pulse provided very noisy traces as shown in Figure 32. However, with some modifications to the set up such as replacing the photodetector with a less-noisy detector, replacing some of the cables, and using index matching gel at the end of the 12 km fiber length to control reflectance, much more stable traces could be achieved as in Figure 33.

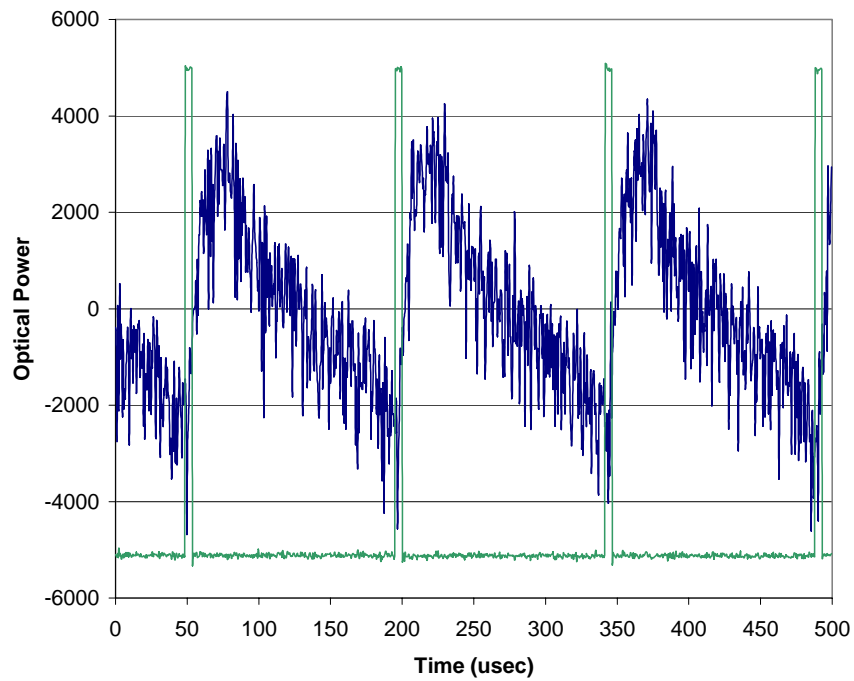


Figure 32. Noisy ϕ -OTDR traces

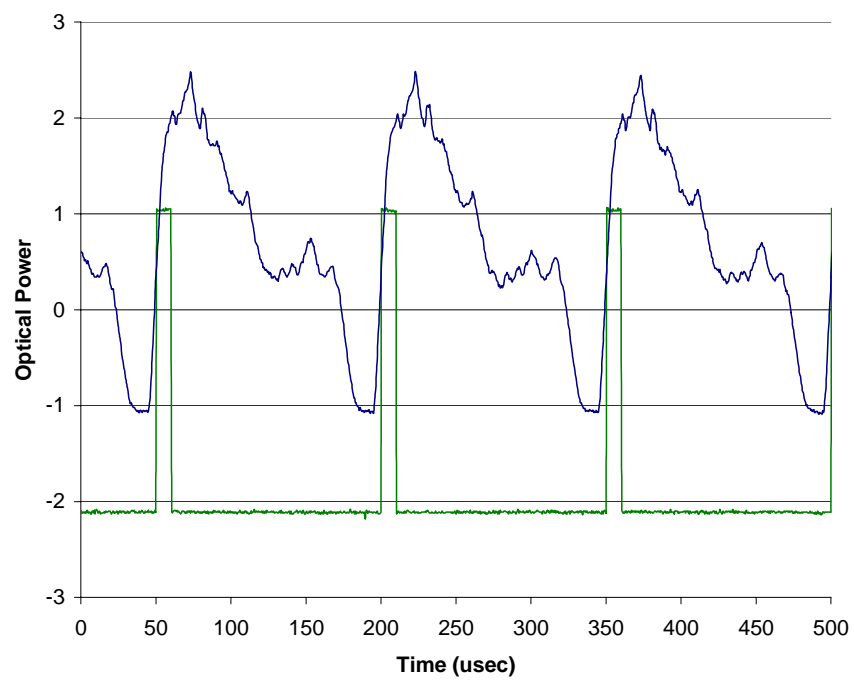


Figure 33. Stabilized ϕ -OTDR traces

Once it was possible to generate stable return pulses, work began in attempting to detect phase disturbances. By modulating the PZT placed at the 2 km point in the path length it was possible to longitudinally stretch the fiber to produce a phase shift that affected the ϕ -OTDR trace at the point in time relative to the laser pulse corresponding to the location of the phase shift.

A LabView program designed to transfer data from the oscilloscope to the computer provided a means to interpret the data collected. The PZT was set to pulse every 300 μsec (i.e. every other return trace) so that a side by side comparison of a pulsed vs. non-pulsed traces could be made. Slight differences could be observed on the oscilloscope, but once the pulses were subtracted from each other and displayed on the computer, disturbances could consistently be observed. Figure 34 shows two successive ϕ -OTDR traces superimposed upon one another, with their difference also plotted. The disturbance peak occurred at the 20 μsec point, which corresponds to the location of the simulated intrusion (2 km). With this data it appeared feasible that a phase disturbance in a long fiber could be detected and located.

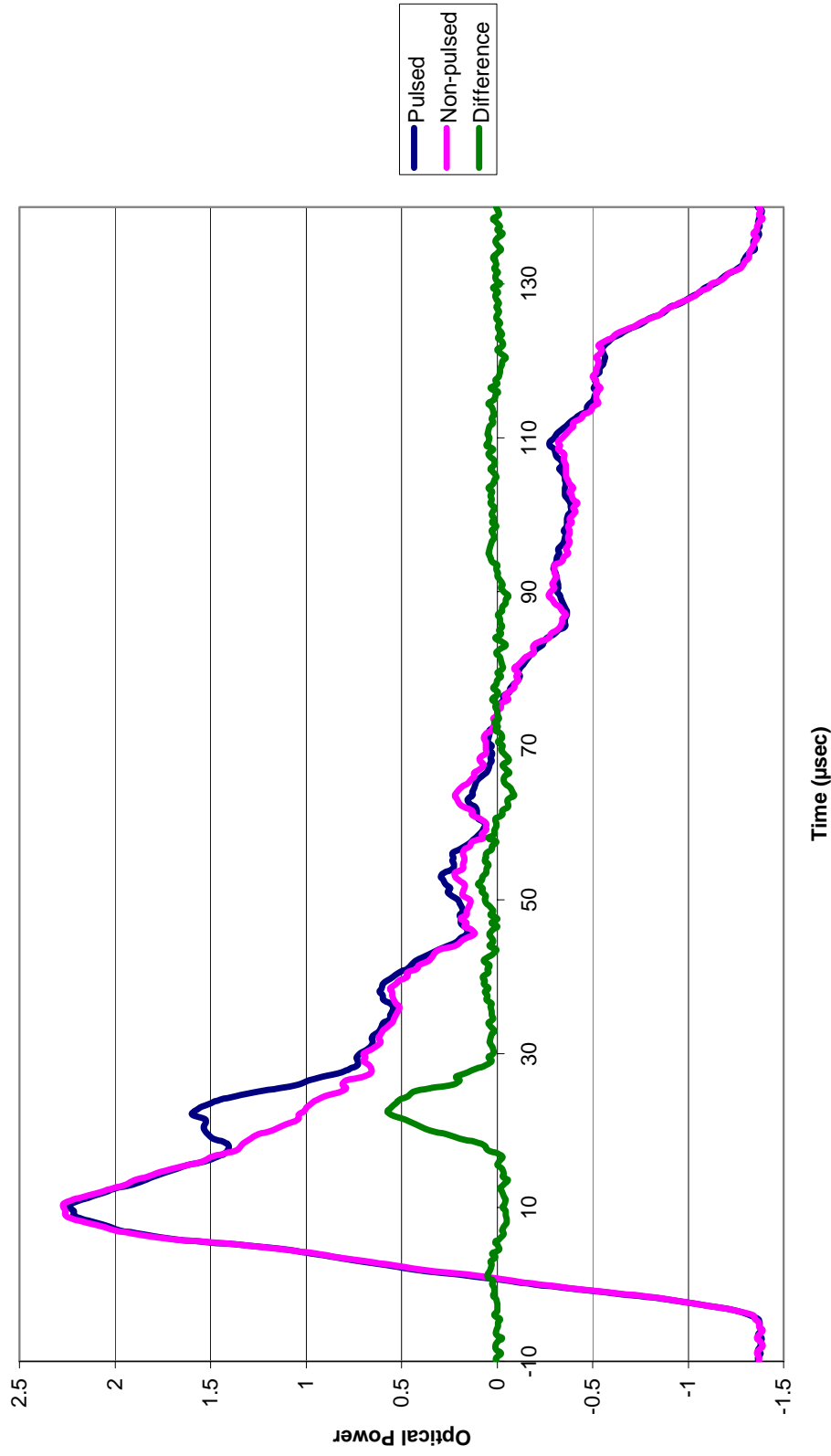


Figure 34. Phase OTDR trace

Once data recorded in the laboratory setting indicated that operation of the sensor was possible, the set up was relocated to Texas A&M's Riverside Campus. At the Riverside facility a ~40 m perimeter of fiber optic cable was buried in a triangular perimeter, as shown in Figure 35, and spliced into the 12 km length of fiber in the laboratory building.

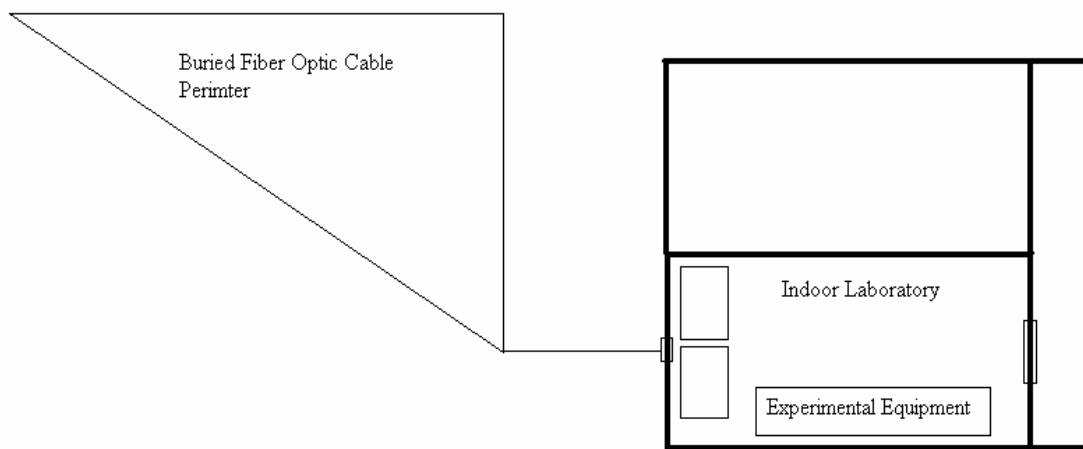


Figure 35. Riverside Campus facility layout

The buried fiber was spliced into the 12 km perimeter by setting it at the similar 2 km point in the path length. The light first passes into the coupler, through the 2 km, then through the buried fiber, and finally down the 10 km. The fiber was buried at a depth of 20 cm on a level, grassy section of land outside the test facility. The ϕ -OTDR set up was recreated and initial readings were taken using the new data acquisition system. Instead of reading the data in as before on the LabView card a new faster (60

MS/s) Gage Instruments data acquisition card with on board memory was utilized so more data points per scan could be registered.

The system behaved much the same as in the laboratory setting. Since the Riverside facility is fairly isolated from the noises and disturbances of the city and university, much more detail in the response to disturbances was noticeable. Whereas before, acoustic disturbances were a non-stop scenario, with the new isolated setting individual noise disturbances were noticeable in the ϕ -OTDR traces. With the laser and 12 km fiber set upon a granite table to suppress vibrational disturbances, “jumps” in the return trace could be seen with speech and walking up to a distance of 20 feet away from the set up. However, even with these effects a stable enough trace was produced to take field measurements.

The first intrusions were conducted by walking along the buried fiber path outside. The data collected showed a steady sequence of phase disturbances correlating with the individual steps along the path. With this success the next intrusions were conducted by driving a car over the perimeter. The traces in Figure 36 and Figure 37 show the ϕ -OTDR trace, and the difference in these traces, respectively, of the car simulation. Substantial peaks could be seen as the tires rolled across the buried fiber. Compared to the walking intrusions, the peaks were orders of magnitude larger, as would be expected with the vast increase in weight.

Thus, the laboratory and field test results indicate that the buried fiber optic sensor is a candidate solution to the low-cost monitoring of multi-km perimeters.

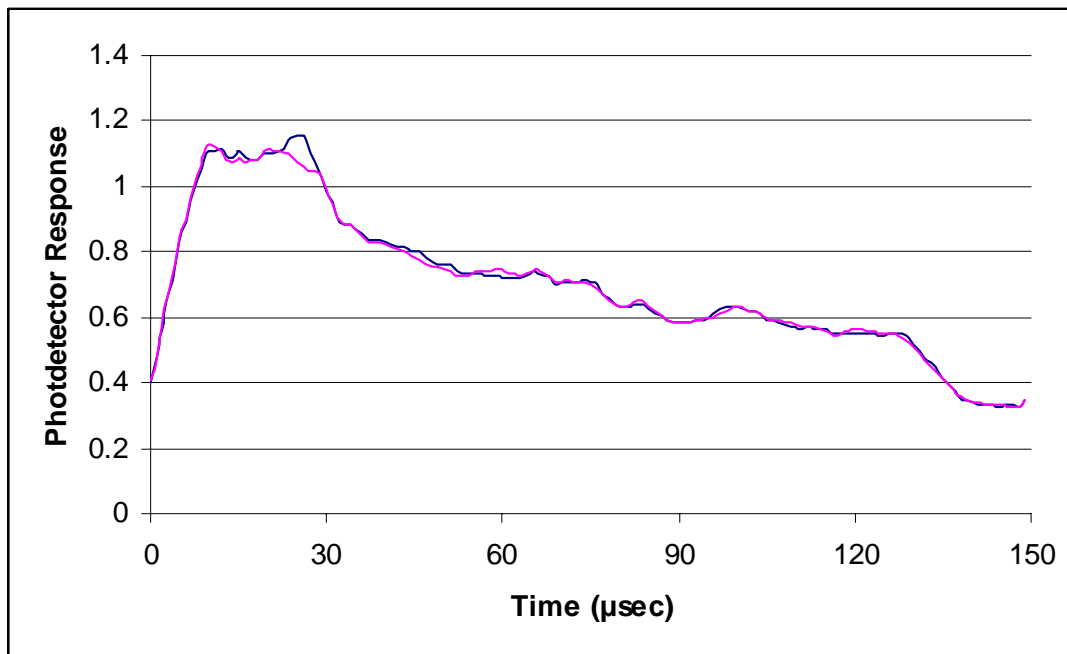


Figure 36. Field test ϕ -OTDR, comparing traces with and without car driving over the buried fiber cable

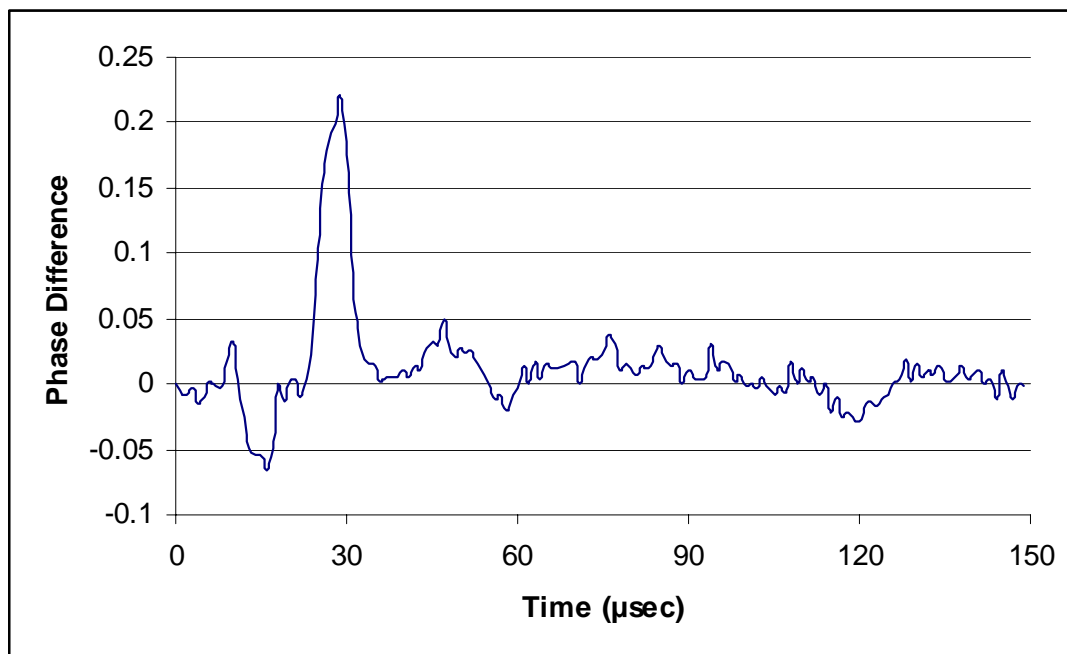


Figure 37. Difference of ϕ -OTDR traces in Fig. 36 showing intrusion peak

CHAPTER V

CONCLUSIONS AND FUTURE WORK

A. Conclusions

Techniques for implementing a buried fiber optic intrusion sensor utilizing an ultra-stable Er: fiber laser in conjunction with a phase sensitive optical time domain reflectometer (ϕ -OTDR) were investigated experimentally. The laser developed for this purpose was heavily insulated against environmental effects as to limit the effects of thermal and acoustic fluctuations. The ϕ -OTDR was successfully demonstrated in the laboratory and in a field test.

Under the most stable environmental conditions, the laser was found to operate in a single longitudinal mode with occasional mode hops. Frequency drift in the laser was monitored simultaneously with two Mach Zehnder interferometers housed in insulated enclosures to minimize environmental effects. The rate of fringe drift in the interferometers reflected a combination of the drift effects from both the laser and the interferometers, and it was assumed that the observed drift was mainly due to the laser. Under the quietest of laboratory conditions the frequency drift approached 1 kHz/s, better than needed for successful operation of the intrusion sensor.

After the laser stability was confirmed, it was possible to focus on the feasibility of producing a ϕ -OTDR intrusion sensor capable of distinguishing phase disturbances in multi-km lengths of fiber. Using a piezoelectric transducer to produce phase

changes at the 2 km point in a 12 km fiber path, the ability not only to detect a disturbance but also to locate it was demonstrated. Finally, the ϕ -OTDR was utilized in a field demonstration to detect and locate intruders walking or driving over the buried fiber optic cable from the pressure-induced phase shift in the fiber. Results from these tests show, at least preliminarily, that intrusions can be detected in buried stretches of fiber optic cable through the use of the ϕ -OTDR system.

B. Future work

Future work on this topic should emphasize further field testing and signal analysis. Laboratory and field test results have proved the feasibility of the ϕ -OTDR intrusion sensor, but extensive field testing is required to show that the sensor can be implemented as a practical technique. The Riverside facility as described in Chapter IV provides a suitable setting for field testing of the intrusion sensor. Preliminary results show the capability to detect intrusions, but further work must go into the stabilization of the system and improving the detection range.

Additionally, work on signal processing is needed. It has been shown in the laboratory that the system can distinguish between varying degrees of phase shift produced in the fiber. This leads to the expectation that, with suitable signal analysis, the system may be able to distinguish between people, vehicles, animals, and environmental disturbances. This step is key to the practical implementation of this

system, as false alarm rates will depend on the ability to distinguish human intruders from animals or environmental disturbances.

Finally, the ability to detect multiple disturbances at the same time can be simulated in the laboratory using multiple PZTs to produce phase shifts at different points in the fiber, and in the field with actual intruders crossing over buried fiber cable. This would provide a better understanding of the practical application of the sensor to perimeter security as the ability to detect simultaneous disturbances along varying points of the perimeter is essential.

This type of sensor might be utilized in areas other than perimeter security as well. For instance, it could be used for instrumenting geological fault lines to monitor seismic disturbances as well as for the early detection of earthquakes. Work in this area would not only monitor the location of interference but also seek to determine the magnitude of the disturbance. Once validated in the field, this system could see countless beneficial uses throughout our world.

REFERENCES

- [1] W. Cornelius, "Death at the border: The efficacy and 'unintended consequences' of US immigration control policy, 1993-2000," Center for Comparative Immigration Studies, Working Paper no. 27, November 2000.
- [2] W. Seo, *Fiber Optic Intrusion Sensor Investigation*, Ph.D. Dissertation, Texas A&M University, College Station, 1994.
- [3] How Stuff Works, "Optical fiber structure." Available: <http://electronics.howstuffworks.com/fiber-optic1.htm>. February 2004.
- [4] Corning Fiber, "Spectral attenuation in a fused silica fiber." Available: www.corningfiber.com. February 2004.
- [5] D.A. Krohm, *Fiber Optic Sensors – Fundamentals and Applications*, Research Triangle Park, N.C., Instrument Society of America, 1998.
- [6] J. Park, *Buried Fiber Optic Sensor*, M.S. Thesis, Texas A&M University, College Station, 1992.
- [7] Corning Cable Systems, "Basic principles of fiber optics", www.corningcablesystems.com/web/college/fibertutorial.nsf/ofpara?OpenForm. 29 Jan 2004.
- [8] C. H. Henry, "Theory of the linewidth of semiconductor lasers," *IEEE Journal of Quantum Electronics*, vol. QE-18, pp.259-264, Feb. 1982.

- [9] R.L. Byer, "Experiment 5: Erbium doped fiber amplifier and laser."
<http://www.stanford.edu/class/appphys304/coursework/Experiment%205/EXP5.pdf>, 21 Jan 2004.
- [10] L. Kazovsky, S. Benedetto, and A Willner, *Optical Fiber Communication Systems*, New York: Artech House, 1996.
- [11] E. Desuvire, *Erbium-Doped Fiber Amplifiers*, New York: John Wiley & Sons Inc. 1994.
- [12] M. K. Barnoski and S. M. Jensen, "Fiber waveguides: A novel technique for investigating attenuation characteristics," *Appl. Opt.*, vol. 15, pp. 2112-2115, 1976.
- [13] B. Costa, B. Sordo, U. Menaglia, L. Piccari and G. Grasso, "Attenuation measurements performed by backscattering technique," *Electron. Lett.*, vol.16, pp. 352-353, 1980.
- [14] M. K. Barnoski, M. D. Rourke, S. M. Jensen, and R. T. Melville, "Optical time domain reflectometer," *Appl. Opt.*, vol. 16, pp. 2375-2380, 1977.
- [15] K. N. Choi and H. F. Taylor, "Spectrally stable Er-fiber laser for application in phase-sensitive optical time domain reflectometry," *IEEE Photon. Technol. Lett*, vol. 16, pp. 386-388, 2003.
- [16] K. N. Choi, J. C. Juarez, and H. F. Taylor, "Distributed fiber optic pressure/seismic sensor for low-cost monitoring of long perimeters," SPIE Conference 5090, AeroSense 2003, Orlando, FL, April 2003.

APPENDIX A

EQUIPMENT USED

Oscilloscope: Tektronix 11201A Digitizing Oscilloscope

Photodetector: ThorLabs D400FC InGaAs Detector

Fiber: Corning SMF28

Couplers: FIS Singlemode 3 dB coupler SMF28 1550nm

Amplifier: Keopsys Fiber Amplifier

Data Acquisition Card: National Instruments BNC 2110

Pulse Generator: Tektronix PG501 Pulse Generator

Function Generator: Hewlett Packard 3325B

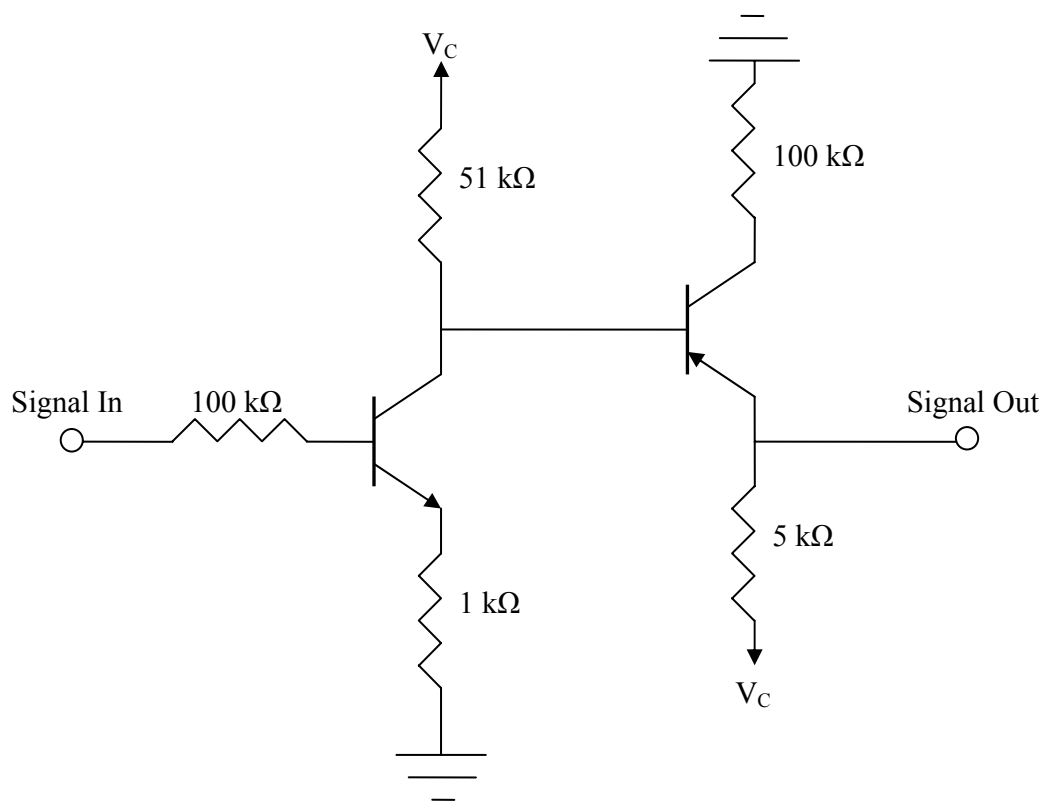
PZT: APC International 42-1080

Low Noise Amplifier: Stanford Research Systems SR560

Current Source: ILX Lightwave LDX-3207B

APPENDIX B

AMPLIFIER CIRCUIT



VITA

Eric William Maier was born on June 30, 1980 in Atlanta, Georgia to parents Stephen and Catherine Maier. He has one brother, Bryan Maier, and was married in 2002 to his wife, Jennifer. He received his Bachelor of Science degree in electrical engineering from Texas A&M in May of 2002 and received his Master of Science in electrical engineering in May of 2004. His area of focus was optical engineering during his course of study at Texas A&M.

Permanent Address:

1323 Alto Dr.

Richardson, TX 75081

The typist for this thesis was Eric William Maier.